
Fatty acid isotopic fractionation in the diatom *Chaetoceros muelleri*

Remize Marine ^{1,2,*}, Planchon Frederic ¹, Loh Ai Ning ², Le Grand Fabienne ⁵,
Mathieu-Resuge Margaux ^{1,3}, Bideau Antoine ¹, Corvaisier Rudolph ⁵, Volety Aswani ⁴,
Soudant Philippe ^{5,*}

¹ Univ Brest, CNRS, IRD, Ifremer, UMR 6539 LEMAR, F-29280 Plouzané, France

² University of North Carolina Wilmington, Department of Earth and Ocean Sciences, Center for Marine Science, 5600 Marvin K. Moss Ln, Wilmington, NC 28403, USA

³ WasserCluster Lunz – Inter-University Centre for Aquatic Ecosystem Research, Dr. Carl Kupelwieser Promenade 5, A-3293 Lunz am See, Austria

⁴ Elon University, 50 Campus Drive, Elon, NC 27244, USA

⁵ Univ Brest, CNRS, IRD, Ifremer, UMR 6539 LEMAR, F-29280 Plouzané, France

* Corresponding authors : Marine Remize, email address : marine.rem@hotmail.fr ; Philippe Soudant, email address : philippe.soudant@univ-brest.fr

Abstract :

Carbon isotopic fractionation was studied during the development of the diatom *Chaetoceros muelleri* grown in batch culture with ¹³C-depleted CO₂ addition. Cellular and growth parameters and isotopic composition of dissolved inorganic carbon and particulate organic carbon were monitored every two days, while the content and isotopic composition of individual fatty acid in polar lipid and neutral lipid were measured on the 5th day (end of exponential phase), 10th and 14th days (stationary phase). Continuous addition of petrochemical CO₂ to the algae led to a rapid and strong modification of dissolved inorganic carbon isotopic composition with cascading effects on particulate organic carbon and fatty acid isotopic compositions. Carbon isotope fractionation in *Chaetoceros muelleri* ranged from 17‰ to 25‰ and changed according to culture ages. Isotopic fractionation into fatty acids, overall, was similar between polar and neutral lipids, and was systematically higher than in particulate organic carbon. At the end of the exponential growth phase, the isotopic composition of individual fatty acids varied from -51.3‰ to -58.4‰. At this culture age, large differences in the isotopic compositions between fatty acids were observed. Polyunsaturated fatty acids such as 16:3n-4, 18:4n-3, and 20:5n-3 were more strongly ¹³C-depleted than other fatty acids such as 14:0, 16:0, 16:1n-7 or 18:1n-9. These results showed how isotopic effects occur during the desaturation and elongation phases. Such isotopic effects were also supported by the lower $\delta^{13}\text{C}$ of averaged $\delta^{13}\text{C}$ of saturated fatty acids and monounsaturated fatty acids as compared to those of polyunsaturated fatty acids. However, during the stationary phase, fatty acid isotopic compositions were less variable and closer to particulate organic carbon, while saturated and monounsaturated fatty acids were more depleted than polyunsaturated fatty acids. Our study underlined the importance of consideration of phytoplankton physiological status when conducting ecological and biogeochemical studies as they appeared to strongly control phytoplankton carbon isotopic composition.

Highlights

► *C. muelleri* was grown with petrochemical CO₂ to assess carbon isotope fractionation. ► Fractionation of particulate organic matter varied with culture phases (17–25‰). ► Isotopic composition of individual fatty acids varied from –51.3 to –58.4‰. ► PUFA were more depleted in ¹³C than SFA or MUFA during late exponential phase. ► Differences of carbon fractionation between fatty acids decreased with aging culture.

Keywords : Fractionation, Stable isotopes, Photosynthesis, Phytoplankton, *Chaetoceros muelleri*, Fatty acid synthesis

1. INTRODUCTION

Global oceans and marine ecosystems are currently under significant threats due to increasing levels of atmospheric CO₂ and on-going climate change. At the base of marine ecosystems, phytoplankton groups are diverse and widely distributed and are likely to be impacted by these climatic changes. In response to changes in environmental factors, photosynthetic organisms can modify their physiology and can modulate their productivity. For example, their lipid membrane composition changes with temperature [1-3]. Among phytoplankton taxa of importance at a global scale, diatoms are ubiquitous, found from cold to warm waters, and they account for about half of the global primary production [4]. Any alteration to their distribution, diversity, and production in response to global changes are expected to have tremendous effects on marine ecosystems.

The stable isotopic composition of carbon (ratio of ¹³C vs. ¹²C expressed as δ¹³C against the Vienna Pee Dee Belemnite (VPDB) reference standard) is widely used for studying the on-going changes and their impacts on ecosystem-related processes in the different oceanic carbon pools (inorganic, organic, dissolved, particulate, sedimentary), and has proven to be a useful tracer. For example, the δ¹³C of dissolved inorganic carbon (δ¹³C-DIC) and its recent decrease due to the introduction of CO₂ from fossil fuels with a light isotopic composition (the so-called Suess Effect) have been used to infer quantitative estimates of oceanic uptake of anthropogenic CO₂ (e.g. Gruber and Keeling [5]). This descriptive capability of δ¹³C also concerns the organic carbon pool, which is derived primarily from marine photosynthetic activity. The δ¹³C of bulk particulate organic carbon (δ¹³C-POC), and by extension of any organic compounds synthesized by marine algae (pigments, sugar, proteins, and lipids), provide substantial information on ecosystem dynamics as well as environmental and biogeochemical parameters. However, deciphering this information has proven to be particularly challenging since multiple factors govern the biological fractionation of carbon isotopes.

During photosynthesis, phytoplankton incorporates aqueous CO₂, assumed to be available in excess in the marine environment [6], and converts it into organic carbon. This process preferentially uses the light isotope (¹²C) over the heavy one (¹³C), leading to a progressive depletion of ¹²C relative to ¹³C in the residual aqueous pool. Carbon fixation by ribulose-1,5-biphosphate carboxylase/oxygenase (RUBISCO) and β-carboxylases during photosynthesis is responsible for the strongest isotopic effect [6-8] and varies according to RUBISCO types [9, 10]. Commonly, the RUBISCO fractionation value is assumed to be around 25‰ [11, 12], but this value has been

revisited recently. Fractionation factor by type IA or IB RUBISCO appears to be close to the consensus value of 25‰, while fractionation by type II RUBISCO, occurring in some diatoms, is lower, around 18-20‰ [10].

The factors influencing carbon isotope fractionation in planktonic communities have been investigated through various *in situ* studies [13, 14] as well as from culture experiments performed in batch [15-18] or chemostat [12, 19] and with variable CO₂ levels. The isotopic composition of phytoplankton depends on several factors including the species considered [20-22], the physiological status, the growth rate and the cell size [23]. It is also dependent on the species of inorganic carbon that is assimilated by the alga. In case of limited availability of CO₂, HCO₃⁻ via carbon concentrating mechanisms (CCM) can be used alternatively as a substrate for enzymatic fixation and can change the isotopic composition of organic carbon [7, 24].

Particulate organic carbon of phytoplankton is composed of different types of organic compounds whose signatures can be substantially different. Carbon isotopes are not distributed uniformly among lipids, carbohydrates, and proteins [14, 25, 26]. The lipid fraction is more depleted in ¹³C relative to bulk POC or other main compounds [27, 28]. As for bulk carbon, the isotopic composition of lipids varies according to several factors: the isotopic composition of the carbon source [27, 29], the biosynthetic routes used to produce lipids [28, 30], the lipid classes [30], the compartmentalization of the organelles within the cell [29] and the physiology of phytoplankton [29]. Studying fractionation into lipids can then give further information on the fate of carbon after its enzymatic fixation by RUBISCO.

However, carbon fractionation remains not fully understood and rarely combined with physiological and cellular parameters. Utilizing culture experiments, this study focuses on understanding the processes responsible for carbon isotope fractionation during the development of the diatom *Chaetoceros muelleri* (*Chaetoceros* is one of the most abundant and widespread genera of diatoms). We selected this species because diatoms are responsible for around 50% of the global primary production [4] and thus could be particularly useful in understanding microalgae carbon fractionation in the global ocean. Furthermore, as diatoms are characterized by a high 20:5n-3 content, they are also adequate to study how carbon fractionation is modulated by fatty acid synthesis. The alga was grown with a constant supply of CO₂ of petrochemical origin (i.e, depleted in ¹³C) and monitored for 24 days. Using compounds-specific stable isotope analysis (CSIA), our goal is to resolve the carbon isotope fractionation in individual fatty acids (FA) in comparison with the bulk carbon fractionation during the growth of *C. muelleri*. FA profiles and isotopic signatures have been determined at three time points (5, 10 and 14 days) during the diatom culture.

2. MATERIAL & METHODS

2.1. Culture conditions and experimental strains

Monospecific cultures were conducted with the marine diatom *Chaetoceros muelleri* (strain CCAP 1010/3 obtained from the CCAP culture collection, formerly listed as *Chaetoceros neogracile* VanLandingham 1968). The inoculum came from a preculture in a growing stage (late exponential phase, five days old) and have been monitored in similar conditions as the culture balloons. The inoculum was initially transferred in a filtered sterile natural seawater and implemented with nutrients (Walne's medium) [31]. Cells were grown in batch (2 L balloon) at 19°C under continuous light (white light, 24 hours light cycle, 100 $\mu\text{moles photons m}^{-2}\cdot\text{s}^{-1}$), and CO₂ addition for 24 days. The CO₂ gas (Air Liquide, Bagnoux, France) added to the culture was of petrochemical origin and was strongly depleted in ¹³C ($\delta^{13}\text{C-CO}_2 = -37.7\text{ ‰}$ as measured by a gas bench, cf 2.5). CO₂ was directly added in the culture balloon with a bubbling intensity of five bubbles per second ensuring gentle stirring. The experimental set up was designed to produce a sufficient quantity of biomass, allowing detailed monitoring in triplicates of carbon isotopic composition of both POC and FA during algal growth. To monitor algal CO₂ assimilation, pH was measured at t₀, t₅, t₁₀, t₁₄, t₁₉ and t₂₄ during this study. Three control balloons with no algal inoculum were also followed at t₀ and t₂₄: one was bubbled with the same CO₂ used for the culture balloons, another with air only and the last was not bubbled.

2.2. Sample collection

Sampling for flow cytometry analysis (2 mL) was performed every two days for 24 days for a total of 16 samples. For POC and DIC concentrations and stable isotopic compositions, samples were collected every four days (t₀, t₅, t₁₀, t₁₄, t₁₉ and t₂₄). A volume between 15 mL to 50 mL, depending on cell concentration and to avoid filter saturation, was filtered through pre-combusted 0.7 μm nominal pore-size glass fiber filters (Whatman grade GF/F CAT No.1825-110, Cytiva, France), then dried at 55°C and stored at room temperature until analysis. DIC samples were collected from the filtrate of POC samples. Twelve mL was poured in Exetainer[®] tubes (9RK8W, Labco, Wales, UK), poisoned with 20 μL of HgCl₂, and stored at 4°C until DIC analysis. For FA concentration and isotopic composition, samples were collected at t₀, t₅, t₁₀ and t₁₄. Samples at t₀ were collected from the preculture directly before inoculum of the culture balloons. For FA analysis, twenty mL of culture was filtered on a pre-combusted 47 mm GF/F filter (porosity 0.7 μm), and boiling water was directly added after filtration to stop lipase activity. To extract lipids, the filter was immersed into 6 mL of 2:1 (v:v) chloroform:methanol solvent

mixture until further analysis (at least 24 hours). All extracts were flushed with nitrogen and stored at -20 °C until analysis. At the time as POC and fatty acid samples were collected, the pH was measured using an electronic pH meter with electrodes (pH meter pH-212 Q79955 Voltcraft, Conrad Electronic, Haubourdin, France). For the three control balloons, the pH was only measured at t_0 and t_{24} , beginning and end of the experiment.

2.3. Flow cytometry analysis

Cellular variables were measured using a FACScalibur (BD Biosciences, San Jose, CA, USA) flow cytometer with a 488 nm blue laser, detectors of forward and side light scatter, and three fluorescence detectors: green (525/30 nm), yellow (583/26 nm) and red (680/30 nm). Forward scatter (forward scatter, FSC), side scatter (side scatter, SSC), and red fluorescence (FL3, red emission filter long pass, 680 nm) were used to select the algae population. FSC and SSC inform the relative size and complexity of cells, while red fluorescence is related to cell chlorophyll content.

Two fluorescent probes were used to evaluate viability and lipid content, according to Lelong, et al. [32] and Seoane, et al. [32]. The SYTOX Green (Molecular Probes, Invitrogen, Eugene, OR, USA, at a final concentration of 0.05 μ M) binds to the DNA of a permeable or permeabilized cell and was used to estimate the percentage of dead cells in the culture sample [32]. The BODIPY probe (BODIPY 505/515 FL; Thermo-Fisher Scientific, Waltham, MA, USA, at a final concentration of 10 mM) was used as a proxy of lipid reserves, as it stains lipid droplets within microalgae cells [33]. Cytometric measurements were performed on live samples right after sampling with or without fluorescent probes every two days.

The concentration of bacteria was also monitored during the experiment, according to Seoane, et al. [33], using SYBR®Green (Molecular Probes #S7563, Invitrogen, Eugene, OR, USA). This DNA staining fluorescence probe allows the detection of DNA stained bacteria on the FL1 detector (Green fluorescence). Results are expressed as the concentration of bacteria cells per mL.

2.4. Particulate organic carbon concentration and stable isotope analysis

The filter for POC concentration and isotopic composition was first fumed with hydrochloric acid to remove particulate inorganic carbon, subsampled with a 13 mm punch, and encapsulated for POC concentration and isotopic composition. Analyses were performed using an elemental analyzer (EA, Flash 2000; Thermo Scientific, Waltham, MA, USA) coupled to a Delta V+ isotope ratio mass spectrometer (Thermo Scientific, Waltham, MA, USA) at the Pôle Spectrométrie Océan (PSO, Brest, France). For POC concentration, acetanilide standards were

used for the calibration, and results are reported in $\mu\text{mol.kg}^{-1}$. Carbon isotope ratios are expressed in delta notation ($\delta^{13}\text{C-POC}$) in per mil (‰) as follow:

$$\delta^{13}\text{C}_{\text{sample}} = \left(\frac{\left(\frac{^{13}\text{C}}{^{12}\text{C}} \right)_{\text{sample}}}{\left(\frac{^{13}\text{C}}{^{12}\text{C}} \right)_{\text{std}}} - 1 \right) \times 1000 \quad (1)$$

where $(^{13}\text{C}/^{12}\text{C})_{\text{std}}$ is the ratio of the reference standard Vienna-Pee Dee Belemnite (V-PDB). For $\delta^{13}\text{C-POC}$, raw results obtained from the spectrometer were corrected for mass drift, the blank contribution from the filter. They were scaled to V-PDB using the certified reference material and in-house standards listed in **Table 1**. The overall precision of the method estimated from routine replicates of *in-house* standards was 0.3%.

2.5. Dissolved inorganic carbon concentration and stable isotope analysis

For the DIC concentration and isotopic composition, the sample preparation was made according to Assayag, et al. [34] as follow: 1 mL subsample was added to a mixing tube and flushed with ultra-pure helium to avoid contamination from residual air, then 23 droplets of phosphoric acid were introduced to convert all DIC species into CO_2 [34]. After 15 hours of equilibration time at room temperature, CO_2 and $\delta^{13}\text{C-CO}_2$ were measured in the headspace by Gas Bench coupled to a Delta Plus mass spectrometer from Thermo Scientific, Waltham, MA, USA (GB-IRMS). The raw data were corrected for liquid-gas fractionation and mass bias using in-house standards (Table 1). DIC concentration and isotopic composition are reported respectively in $\mu\text{mol.kg}^{-1}$ and delta notation ($\delta^{13}\text{C-DIC}$) in per mil (‰) on the V-PDB scale.

Table 1: Certified Reference Materials (CRM) and in-house standards used for $\delta^{13}\text{C}$ measurements. $\delta^{13}\text{C}$ of CRM are certified by the International Atomic Energy Agency (IAEA) and Schimmelmann, et al. [35]

Standard description	Nature	Analysis	$\delta^{13}\text{C}(\text{‰})$	SD
IAEA-CH₆	Sucrose ($\text{C}_{12}\text{H}_{22}\text{O}_{11}$)	$\delta^{13}\text{C-POC}$	-10.45	0.03
IAEA-600	Caffeine ($\text{C}_8\text{H}_{10}\text{N}_4\text{O}_2$)	$\delta^{13}\text{C-POC}$	-27.77	0.04
Acetanilide	Acetanilide ($\text{C}_8\text{H}_9\text{NO}$)	$\delta^{13}\text{C-POC}$	+29.53	0.01
CA21 (in-house)	Calcium carbonate (CaCO_3)	$\delta^{13}\text{C-DIC}$	+1.48	
Na₂CO₃ (in-house)	Sodium carbonate	$\delta^{13}\text{C-DIC}$	-6.88	
NaHCO₃ (in-house)	Sodium bicarbonate	$\delta^{13}\text{C-DIC}$	-5.93	
14:0 (methyl ester)	Tetradecanoic acid methyl ester	$\delta^{13}\text{C-FA}$	-29.98	0.02

14:0 (ethyl ester)	Tetradecanoic acid ethyl ester	$\delta^{13}\text{C-FA}$	-29.13	0.03
16:0 (methyl ester)	Hexadecanoic acid methyl ester	$\delta^{13}\text{C-FA}$	-29.90	0.03
16:0 (ethyl ester)	Hexadecanoic acid ethyl ester	$\delta^{13}\text{C-FA}$	-30.92	0.02
18:0 (methyl ester)	Octadecanoic acid methyl ester	$\delta^{13}\text{C-FA}$	-23.24	0.01
18:0 (ethyl ester)	Octadecanoic acid ethyl ester	$\delta^{13}\text{C-FA}$	-28.22	0.01
20:0 (methyl ester)	Eicosanoic acid methyl ester	$\delta^{13}\text{C-FA}$	-30.68	0.02
20:0 (ethyl ester)	Eicosanoic acid ethyl ester	$\delta^{13}\text{C-FA}$	-26.10	0.03

2.5.1. Calculation of CO_2 concentration and $\delta^{13}\text{C-CO}_2$

In addition to measured parameters, concentrations of DIC species (CO_2 and HCO_3^-) and the isotopic composition of CO_2 ($\delta^{13}\text{C-CO}_2$) were obtained by calculation. Concentrations of CO_2 and HCO_3^- were estimated using DIC concentrations, pH, temperature, and salinity via the program CO2.SYS [36] adapted for Excel.

The $\delta^{13}\text{C-CO}_2$ was calculated according to Rau, et al. [37] using $\delta^{13}\text{C-DIC}$ (measured or estimated) and absolute temperature ($T_k = 292 \text{ K}$), which was maintained constant during the experiment [37] as follow:

$$\delta^{13}\text{C}_{\text{CO}_2} = \delta^{13}\text{C}_{\text{DIC}} + 23.644 - \frac{9701.5}{T_K} \quad (2)$$

a. Carbon isotope fractionation factor between bulk POC and CO_2

The fractionation factor (ϵ_P) between aqueous CO_2 and POC was calculated according to Freeman and Hayes [38]:

$$\epsilon_P = \frac{(\delta^{13}\text{C}_{\text{CO}_2}) - (\delta^{13}\text{C}_{\text{POC}})}{1 + \frac{(\delta^{13}\text{C}_{\text{POC}})}{1000}} \quad (3)$$

We performed two estimates of ϵ_P , with two distinct values of $\delta^{13}\text{C-CO}_2$. The first one ($\epsilon_{P,M}$) was based on the measured values of $\delta^{13}\text{C-DIC}$ in the culture medium and the corresponding $\delta^{13}\text{C-CO}_2$ calculated using Eq. 2.

The second value ($\epsilon_{P,TA}$) was based on the isotopic composition of total assimilated DIC ($\delta^{13}\text{C-DIC}_{TA}$) estimated using a mass balance approach. This mass balance approach was motivated by the high levels of biomass (and of POC) that developed due to the external CO_2 supply and which largely exceeded the initial DIC levels of the natural seawater used for preparing the culture. As an example, at t_5 , the initial DIC concentration ($\sim 700 \mu\text{mol.L}^{-1}$) could only explain 7% of the produced POC ($\sim 10500 \mu\text{mol.L}^{-1}$), the remaining 93% ($\sim 9700 \mu\text{mol.L}^{-1}$) thus coming from added petrochemical CO_2 . The isotopic composition of total assimilated DIC ($\delta^{13}\text{C-DIC}_{TA}$) was

estimated conservatively by considering a binary mixing model between the initial DIC stock present in the natural seawater used for preparing the culture (DIC_{sw}) as the first end-member, and the added DIC due to petrochemical CO_2 addition (DIC_{petro}) as second end-member as follows:

$$(\delta^{13}CDIC_{TA}) = f_{DIC,petro} \times (\delta^{13}CDIC_{petro}) + (1 - f_{DIC,petro}) \times (\delta^{13}CDIC_{sw}) \quad (4)$$

With $\delta^{13}C-DIC_{sw}$, the isotopic composition of the initial seawater measured at day 0 and $\delta^{13}C-DIC_{petro}$ the isotopic composition of DIC deriving from petrochemical CO_2 addition after gas and acid-base equilibration. For $\delta^{13}C-DIC_{petro}$, the $\delta^{13}C-DIC$ measured at the end of the experiment (after 24 days of continuous CO_2 addition) was assumed to be representative of this end-member. The $f_{DIC,petro}$, the molar fraction of petrochemical DIC assimilated by the algae, was estimated using a POC mass balance:

$$f_{DIC,petro} = \frac{([POC]_i - [POC]_0) - [DIC]_0}{[POC]_i - [POC]_0} \quad (5)$$

With $[POC]_i$ and $[POC]_0$, the respective POC concentrations at the time i and 0 and $[DIC]_0$ the initial DIC concentration before CO_2 addition.

2.5.2. Cell and particulate organic carbon growth rates

Algal growth rates were estimated at late exponential growth phase using two different parameters: from the cell concentrations according to Salvesen, et al. [39] and noted μ_{cell} and from the POC and noted μ_{POC} [22].

$$\mu_{cell} = \frac{\ln \left(\frac{[alg]_i}{[alg]_{i-1}} \right)}{(t_i - t_{i-1})} \quad (6)$$

With, $[alg]_i$ the algal concentration at time i (t_i) and $[alg]_{i-1}$ algal concentration at time $i-1$ (t_{i-1})

$$\mu_{POC} = \frac{\ln [POC]_{i+1} - \ln [POC]_i}{t_{i+1} - t_i} \quad (7)$$

With $[POC]_{i+1}$ POC concentration at time $i+1$ (t_{i+1}) and $[POC]_i$ the POC concentration at time i (t_i).

2.6. Analyses of fatty acids concentration and isotopic composition

2.6.1. Separation of neutral and polar lipids

Lipid extracts were separated into neutral and polar lipids following the method of Le Grand, et al. [40]. Briefly, after sonication, 3 mL of total lipid extract was evaporated with nitrogen, recovered with three washes using chloroform:methanol (final volume 1.5 mL, 98:2 v:v) and spotted at the top of a silica gel column (40 mm x 4mm, silica gel 60A 63-200 μm rehydrated with 6% H_2O , 70-230 mesh, Sigma-Aldrich, Darmstadt, Germany).

The neutral lipid fraction (NL) was eluted using chloroform:methanol (10 mL 98:2 v:v) and the polar lipid fraction (PL) with methanol (20 mL). Both fractions were then collected in glass vials, and an internal standard (C23:0, 2.3 µg) was added. NL and PL fractions were then stored at -20°C until further analysis.

2.6.2. Transesterification to fatty acid methyl esters

Using the protocol described in Mathieu-Resuge, et al. [41], fatty acids were transesterified to fatty acids methyl esters (FAME). Briefly, transesterification was realized by adding 0.8 mL of H₂SO₄/methanol mixture to the lipid extract and heated at 100°C for 10 min. Hexane (0.8 ml) and distilled water saturated in hexane (1.5 mL) were added. The aqueous phase (lower phase, MeOH-water) was deleted after two homogenization and centrifugation. The hexane phase containing FAME was washed two more times with 1.5 mL of distilled water and stored at -20°C until further analysis. Before compound-specific isotopic analysis, samples were concentrated in 100 µL vials.

2.6.3. Fatty acids analysis by Gas Chromatography Flame Ionisation Detector (GC-FID)

Analysis of FAME was performed on a Varian CP-8400 gas chromatograph (Agilent, Santa Clara, CA, USA) by two simultaneous separations on a polar column (DB-WAX: 30 m x 0.25 mm ID x 0.25 µm, Agilent, Santa Clara, CA, USA) and on an apolar column (DB-5: 30 m x 0.25 mm ID x 0.25 µm, Agilent, Santa Clara, CA, USA). The temperature program used was the following: first, initial heating to 0 from 150°C at 50°C.min⁻¹, then to 170°C at 3.5 °C.min⁻¹, to 185°C at 1.5 °C.min⁻¹, to 225 at 2.4°C.min⁻¹ and finally to 250°C at 5.5°C.min⁻¹ and maintained for 15 min. Two µL were injected for each GC-FID analysis.

The FAME were identified by comparison of their retention time with commercial standards (Supelco 37 component FAME mix, the PUFA No.1 and No.3 and the Bacterial Acid Methyl Esther Mix from Sigma-Aldrich, Darmstadt, Germany) and in-house standards mixtures. FA concentrations were reported as mgC.L⁻¹ and as % of total fatty acids from each lipid fraction.

2.6.4. Fatty acids compound-specific isotope analysis

Compound specific isotope analyses (CSIA) of FAME were performed using protocol by Mathieu-Resuge, et al. [41]. CSIA analyses were made on a Thermo-Fisher Scientific (Waltham, MA, USA) GC ISOLINK TRACE ULTRA using the same polar column as for FAME analysis by GC-FID (DB-WAX: 30 m x 0.25 mm ID x 0.25 µm, Agilent, Santa Clara, CA, USA). Only the eleven fatty acids with the highest concentrations (14:0, 16:0,

16:1n-7, 16:3n-4, 18:1n-9, 18:1n-7, 18:2n-6, 18:3n-6, 18:4n-3, 20:4n-6 and 20:5n-3) were selected for compound-specific isotopic analysis, the others presenting too low voltage amplitudes to allow precise stable isotope measurement (i.e, amplitudes < 800 mV and concentration < 100 $\mu\text{gC.L}^{-1}$) were not considered. However, exceptions were made for three fatty acids (18:1n-9, 18:1n-7 and 16:3n-4 in the NL fraction) despite presenting amplitudes lower than 800 mV in this fraction. Unfortunately, all FA attributed to bacteria were below these thresholds.

As for $\delta^{13}\text{C-POC}$ and $\delta^{13}\text{C-DIC}$, $\delta^{13}\text{C-FA}$ was reported in delta notation (δ) expressed in per mil (‰) against V-PDB standard. Calibration to the V-PDB scale was performed using a mix of eight acid ethyl and methyl esters (14:0, 16:0, 18:0 and 20:0, with $\delta^{13}\text{C-FA}$ values ranging from $-26.98 \pm 0.02\text{‰}$ to $-30.38 \pm 0.02\text{‰}$) and supplied by Indiana University Stable Isotope Reference Materials as described in Mathieu-Resuge, et al. [41] (Table 1). The analytical error and analytical precision were 0.2‰ and <0.2‰, respectively, as previously measured by Mathieu-Resuge, et al. [41]. Accordingly, the standards were run at the start of the analytical sequence and also after every three samples for quality control and isotope correction of fatty acid isotopic signature in samples.

2.6.5. Correction of $\delta^{13}\text{C-FA}$ due to trans-esterification

Corrections of $\delta^{13}\text{C-FA}$ values have been made according to the method described in Mathieu-Resuge, et al. [41] and using the following equation:

$$(\delta^{13}\text{C}_{\text{methanol}}) = -n \times (\delta^{13}\text{C}_{\text{FA}}) + (n + 1) \times (\delta^{13}\text{C}_{\text{FAME}}) \quad (8)$$

Where n is the number of carbon atoms in the free FA. The average $\delta^{13}\text{C}$ -methanol value used in this correction (-39.6‰) was estimated by Mathieu-Resuge, et al. [41].

2.6.6. Comparison of fatty acids isotopic composition with bulk particulate organic carbon

To compare fatty acid isotopic composition ($\delta^{13}\text{C-FA}$) and POC isotopic composition ($\delta^{13}\text{C-POC}$), we defined $\Delta_{\text{FA-POC}}$ as follow:

$$\Delta_{\text{FA-POC}} = \delta^{13}\text{C}_{\text{FA}} - \delta^{13}\text{C}_{\text{POC}} \quad (9)$$

2.6.7. Isotopic composition of classes of fatty acids and total fatty acids

Weighted average carbon isotopic signatures ($\delta^{13}\text{C-FA}_{WA}$) were calculated for the different classes of fatty acids (SFA, MUFA, PUFA) as well as n-3 and n-6 PUFA, and total neutral lipids (TNL) and total polar lipids (TPL) using the following equation

$$(\delta^{13}\text{CFA}_{WA}) = \frac{\sum_i^n (\delta^{13}\text{CFA}_i) \times [\text{FA}]_i}{\sum_i^n [\text{FA}]_i} \quad (10)$$

Where $\delta^{13}\text{C-FA}_i$ and $[\text{FA}]_i$ are the isotopic composition and massic concentration (mgC.L^{-1}) of fatty acid i .

2.6.8. Statistical analysis

To assess the potential effect of time and difference between replicates during algae development, ANOVA or PERMANOVA analysis were conducted on the FA mass percentages separately in NL and PL, FA isotopic composition and $\Delta_{\text{FA-POC}}$. Principal component analysis (PCA) coupled with similarity percentage analysis (SIMPER) was used to identify fatty acids that were the main responsible for the overall observed variability (80%). Spearman test was also conducted on fatty acids abundance in both PL and NL to explore the relationship between fatty acids. Pairwise Student tests were used to compare isotopic composition between lipid fraction and between FA. All statistical analyses were performed using R software [42].

3. RESULTS

3.1. Measurement of pH

During *C. muelleri* growth, pH varied from 6.88 ± 0.03 to 7.24 ± 0.01 . The pH of the culture medium was the highest at t_5 with 7.81 ± 0.01 . The pH of the control balloon bubbled with CO_2 remained stable at 6.94 during the experiment while the no bubbling control also stayed relatively constant around 7.72 (7.67 at t_0 and 7.71 at t_{24}). The pH of control bubbled with air was the most variable and increased slightly during the experiment from 7.77 to 7.86 in 24 days.

3.2. Growth parameters

The growth of *Chaetoceros muelleri* was divided into 3 phases according to cell abundance/concentration (Figure 1): (i) an initial and exponential growth phase from t_0 to t_5 (Phase I), (ii) a stationary phase between t_5 and t_{14} (Phase II) and finally (iii) a decline phase from t_{14} until the end (t_{24}) (Phase III). During Phase I, cell

concentration increased rapidly (Figure 1A), from 7.3×10^4 to 1.2×10^7 cells.mL⁻¹ on average for the three replicates corresponding to a mean cellular growth rate of 0.44 d^{-1} (doubling time 1.56 d).

During Phase II, cell concentration remained high and relatively stable, around 1.30×10^7 cells.mL⁻¹ until t_{14} . After t_{14} (Phase III), cell concentration decreased down to 9×10^6 cells.mL⁻¹ with a concomitant increase in bacteria concentration. Bacteria concentration was, on average, three times higher than algal cell concentration during Phase I and around 17 times higher during Phase III (Figure 1B).

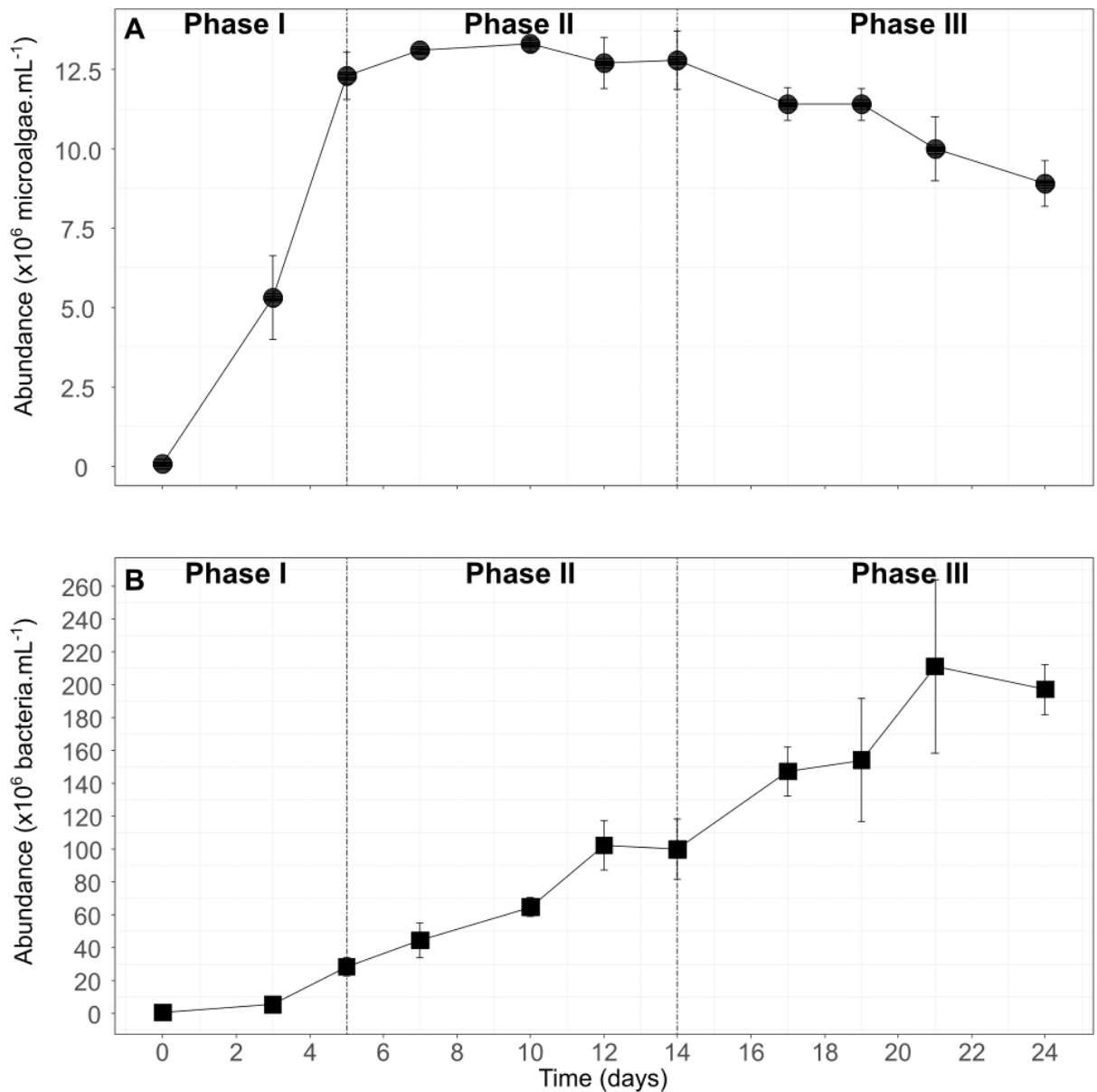


Figure 1: Growth of *Chaetoceros muelleri* (●) [A] and associated bacterial development (■) [B]. The vertical lines define the different growth phases of *C. muelleri*: Phase I (t_0 - t_5), Phase II (t_5 - t_{14}), Phase III (t_{14} - t_{24}). The standard deviations (\pm SD) show the variability between culture replicates ($n=3$).

3.3. Physiological parameters

Cell size and complexity (estimated from FSC and SSC) decreased from 93 to 74 a.u and 22 to 9 a.u, respectively, during the first five days (Phase I) and then rose slowly to 82 a.u and 17 a.u respectively till day 14 (Phase II). During Phase III (day 14 till day 23), FSC ranged between 62 and 83 a.u. and SCC between 12 and 19 a.u. (Table 2). Cell viability remained high between 92 and 97% for the whole duration of the culture (Table 2).

Without taking into account t_0 reflecting the chlorophyll level of the preculture cells, chlorophyll content (FL3 fluorescence) had a decreasing trend during the entire experiment from 16 to 7 a.u. The highest level of chlorophyll was observed at the end of the exponential growth phase (at t_5). The highest NL content estimated by BODIPY staining (green fluorescence on FL1) was observed during Phase II at t_{19} with 473 a.u. while the lowest value was visible at t_3 (in average 50 a.u) (Figure 2).

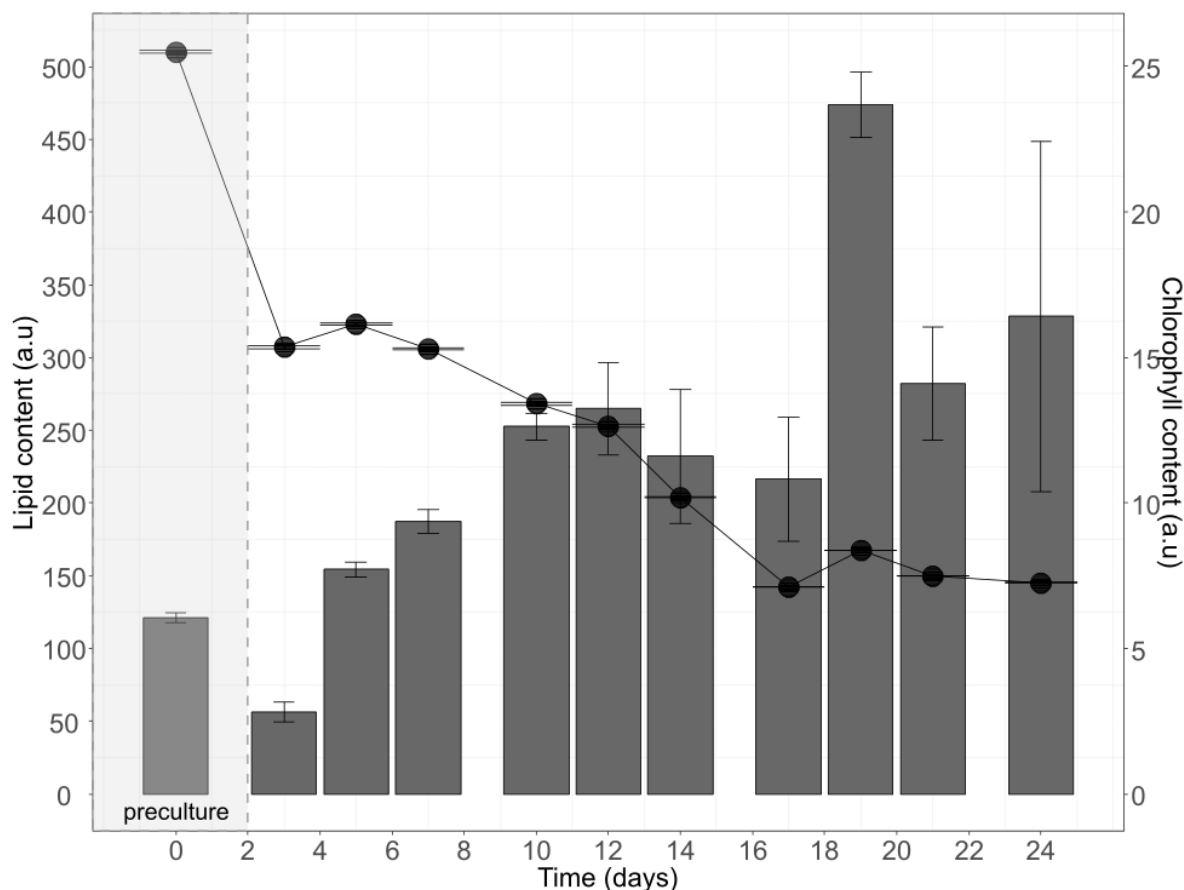


Figure 2: Temporal dynamics of neutral lipid content (estimated by BODIPY staining, barplot) and chlorophyll content as proximate by FL3 fluorescence (line plot). Error bars refer to standard deviations (\pm SD) between culture replicates (n=3). Values collected for t_0 reflect the characteristics of the preculture cells.

Table 2: Temporal dynamics of *C. muelleri* morphological and viability parameters during culture. Results are expressed as Mean \pm SD (n=3). FSC=Forward Scatter; SSC=Side Scatter

Time (days)	FSC	SSC	% of live cells
0*	93.07 \pm 2.63	21.69 \pm 2.21	91.91 \pm 2.00
3	64.23 \pm 1.19	6.93 \pm 0.21	94.39 \pm 3.14
5	74.22 \pm 1.54	9.03 \pm 0.39	97.23 \pm 1.09

7	77.43 ± 1.69	11.71 ± 0.05	96.94 ± 1.83
10	79.83 ± 1.95	14.19 ± 0.17	96.68 ± 2.48
12	81.00 ± 2.23	15.78 ± 0.14	96.48 ± 2.20
14	82.94 ± 2.29	17.01 ± 0.26	96.79 ± 1.96
17	62.56 ± 1.32	12.90 ± 0.30	94.43 ± 2.23
19	68.41 ± 1.03	15.88 ± 0.31	96.55 ± 2.09
21	45.06 ± 0.83	12.78 ± 0.27	96.74 ± 2.01
24	68.52 ± 0.61	19.57 ± 0.19	96.27 ± 2.07

*at t_0 , cellular characteristics were those of preculture cells.

3.4. Dissolved inorganic carbon concentration and isotopic composition

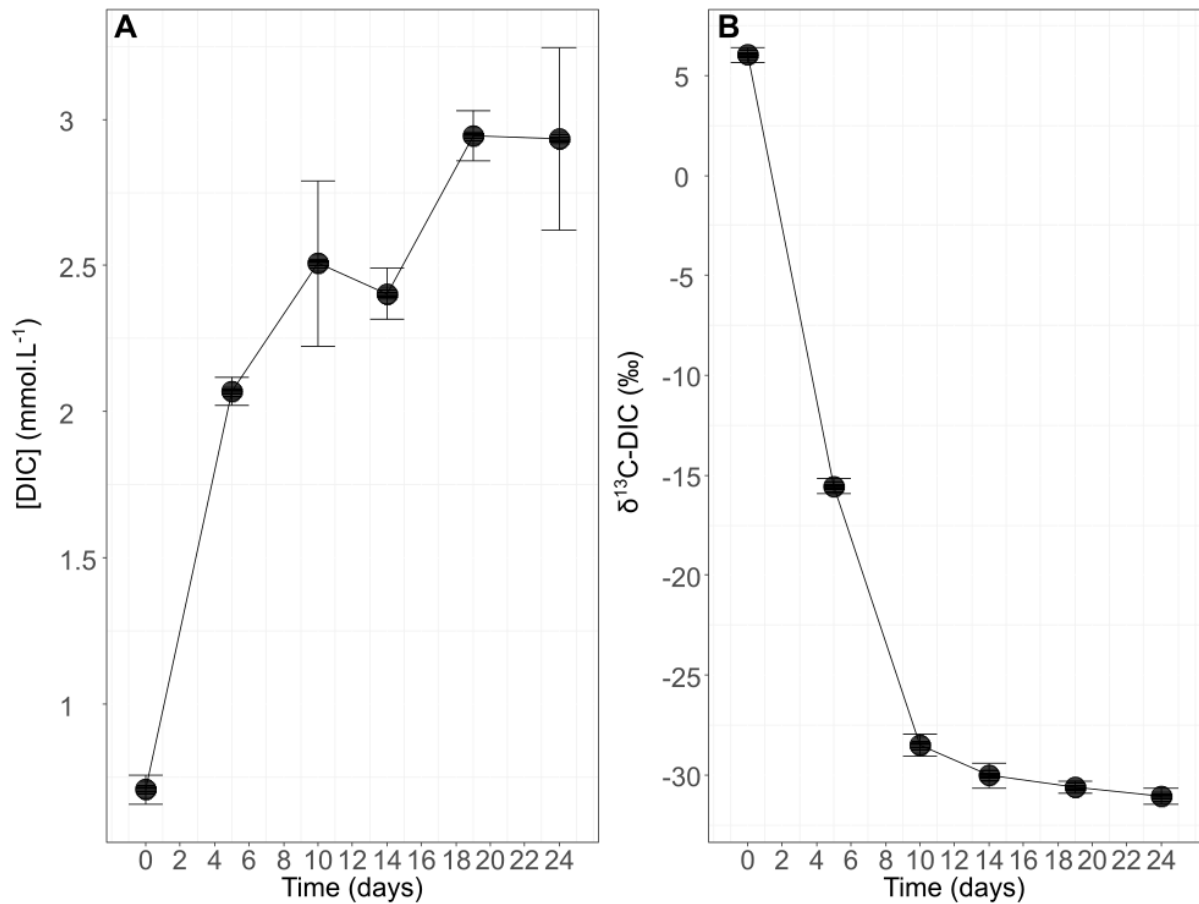


Figure 3: Temporal dynamics of dissolved inorganic carbon concentration [A] and isotopic composition [B] of *C. muelleri*.

Results are expressed as mean ± SD (n=3)

DIC concentration increased from 0.7 to 2.9 mmol.L⁻¹ during the 24 days of the experiment. The final DIC concentration tended to reach a plateau of around 2.9 mmol.L⁻¹ (Figure 3A). δ¹³C-DIC decreased rapidly during Phase I from 6.0‰ to -15.5‰, then stabilized at -29.3‰ during Phases II and III (Figure 3B).

3.5. Particulate organic carbon concentration and isotopic composition

During Phase I, POC concentrations increased rapidly from 1.5 to 22.0 mmol.L⁻¹ (Figure 4A) and reached a plateau during Phase III around 22.3 mmol.L⁻¹. $\delta^{13}\text{C}$ -POC also showed variations during the culture with a rapid and consistent decrease during Phase I of 36‰ in 5 days from -12.9‰ to -48.7‰ (Figure 4B). During Phases II and III, *C. muelleri* isotopic composition kept decreasing and reached a minimum value of -57.0‰ at t₂₄. The carbon quota of the cell (i.e, the C content per cell) increased continuously from t₅ to t₂₄, indicating a progressive accumulation of organic carbon by cells. Values for t₀ were not shown as they corresponded to preculture cells. Algae cells exhibited a mean final C quota of 2.4 pmolC.cells⁻¹ (Figure 4C).

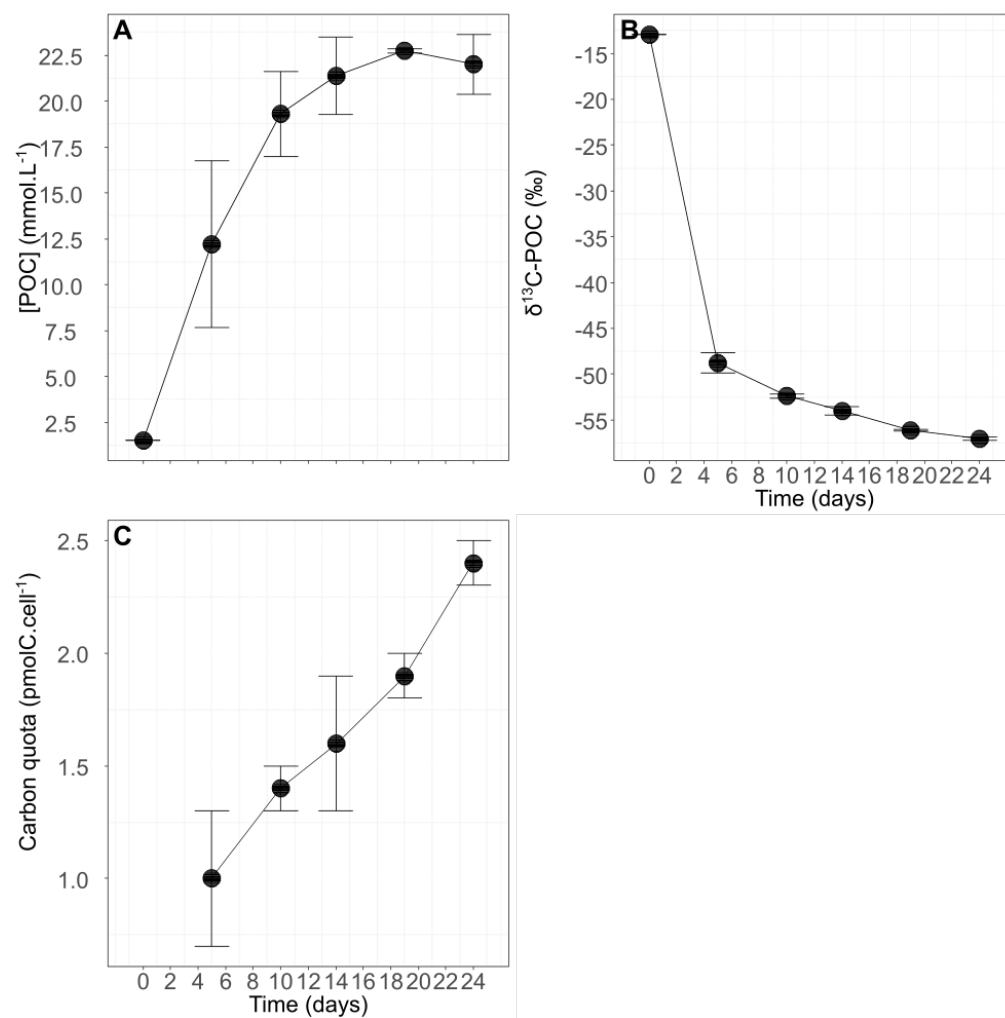


Figure 4: Dynamics of particulate organic carbon concentrations [A], particulate organic carbon isotopic composition [B] and carbon quota [C] for *C. muelleri*. Results are expressed as Mean \pm SD (n=3). t₀ value for carbon quota was not shown as they corresponded to preculture cells.

3.6. Isotopic fractionation between CO₂ and bulk particulate organic carbon

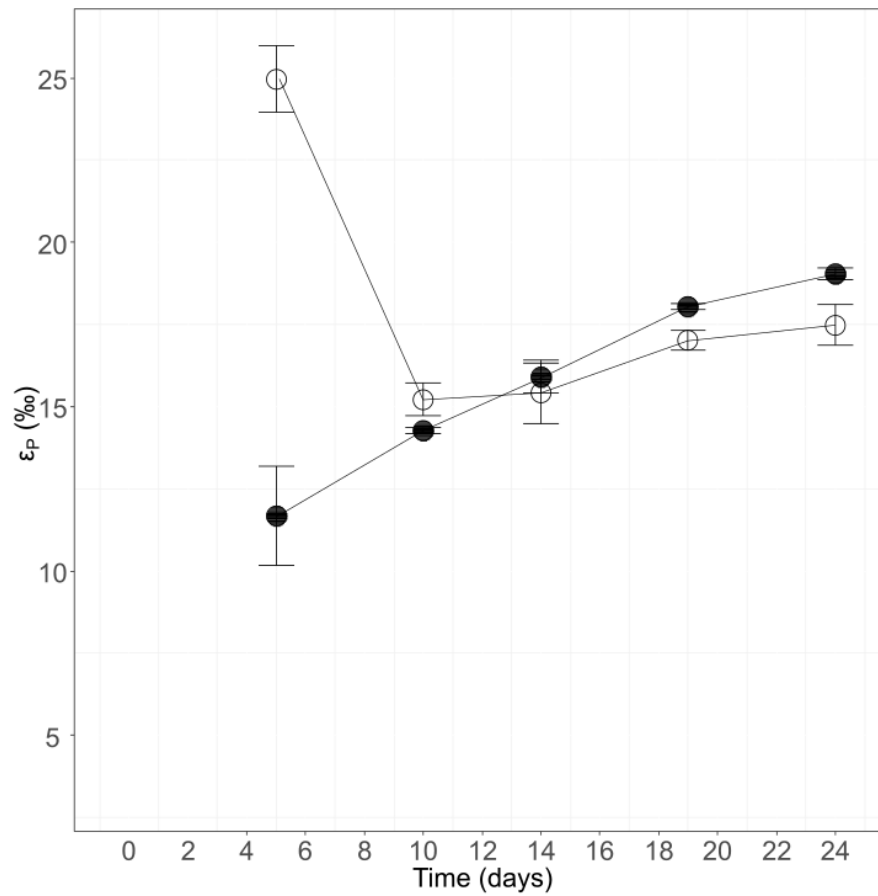


Figure 5: Temporal dynamics of isotopic fractionation between CO₂ and bulk particulate organic carbon deduced from measurement and total assimilated dissolved inorganic carbon (respectively $\epsilon_{P,M}$ (solid line opened dot) and $\epsilon_{P,TA}$ (solid line filled dot)). Results are expressed as Mean \pm SD (n=3).

Fractionation factors (ϵ_P) varied during the experiment and substantially according to the $\delta^{13}\text{C-CO}_2$ chosen as reference (Figure 5). The highest value (24.9‰) was observed for $\epsilon_{P,M}$, at the end of Phase I (t_5). Then, it decreased during Phase II (mean value of 15.3‰) and finally slightly increased during Phase III to reach 17.2‰. The fractionation factor calculated versus total assimilated DIC ($\epsilon_{P,TA}$) was 11.7‰ at the end of Phase I. Then, it presented a similar temporal dynamic to $\epsilon_{P,M}$, increasing steadily during Phases II and III reaching 19.0‰.

3.7. Content and percentage of fatty acids in neutral and polar lipid fractions.

A total of 50 FA were identified, with 35 of them being in low amounts (less than 1% of the total fatty acids). Total fatty acids in neutral lipid fraction (TNL) varied between $0.8 \pm 0.04 \text{ mg.L}^{-1}$ at t_0 to $66.3 \pm 8.9 \text{ mg.L}^{-1}$ at t_{14} . In comparison, total fatty acids in polar lipid fraction (TPL) increased from $3.2 \pm 0.2 \text{ mg.L}^{-1}$ to $17.1 \pm 0.6 \text{ mg.L}^{-1}$ in Phase I (between t_0 and t_5) and then remained relatively constant between Phase I (t_5) and Phase II (t_{14}) (in

average 18.1 mg.L^{-1}) (Figure 6 **Erreur ! Source du renvoi introuvable.**). PL fraction was dominated by polyunsaturated fatty acids (PUFA), and their proportion relative to TFA decreased with time (from 49% at Phase I (t_5) to 37% at Phase II (t_{14})). In the NL fraction, saturated fatty acids (SFA) were the most important FA category with increasing proportion with time (43% at Phase I (t_5) to 50% at the end of Phase II (t_{14})) inversely to PUFA. In both fractions, PUFA decreased in favor of monounsaturated fatty acids (MUFA) and SFA. BACT (bacterial fatty acids) remained below 1.5% in NL and below 1% in PL between Phase I (t_5) and the end of Phase II (t_{14}) (Table 3). Interestingly, the proportion of BACT increased with time in PL (0.5 to 0.9%) and paralleled the increase of bacterial concentration, as shown in Figure 1.

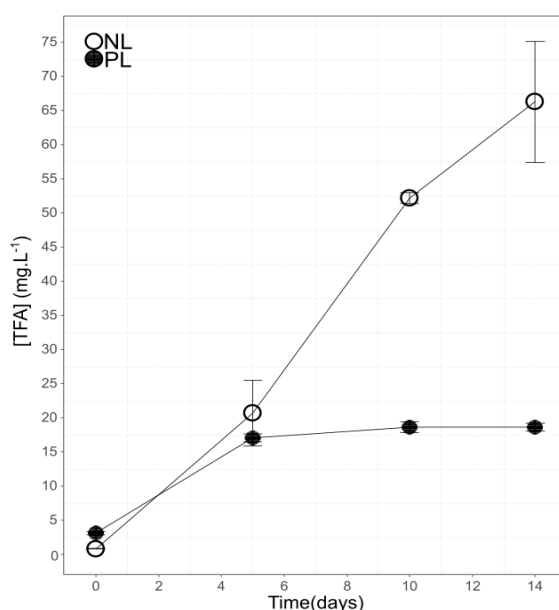


Figure 6: Temporal dynamics of total fatty acids (TFA) concentrations (in mg.L^{-1}) in neutral (NL – opened dots) and polar (PL – filled dots) fraction for *Chaetoceros muelleri*. Results are expressed as Mean \pm SD ($n=3$).

For the PL and NL fractions, the primary FA were 14:0, 16:0, 16:1n-7, and 20:5n-3. As for PUFA, 20:5n-3 proportion decreased with time in both PL and NL. The highest proportions of 20:5n-3 were observed at Phase I (PL: 34% and NL: 9.4%) (Figure 7). Within SFA, proportions of 14:0 in both NL and PL decreased with culture age while 16:0 increased. The main MUFA, 16:1n-7, increased in both NL and PL with age and exponentially during Phase I. 18:1n-9 and 18:1n-7 were low in NL and decreased with age while they were higher and drastically increased in PL between t_5 and t_{14} . The C₁₆ PUFA and C₁₈ PUFA were always higher in PL than in NL, with C₁₆ PUFA decreasing in both fractions with culture age while, on the contrary, C₁₈ PUFA increased. 20:4n-6, 20:5n-3 and 22:6n-3 were much higher in PL than in NL. 20:4n-6 decreased with culture age while 20:5n-3 decreased. 22:6n-3 remained stable in both NL and PL during culture growth.

ONL●PL

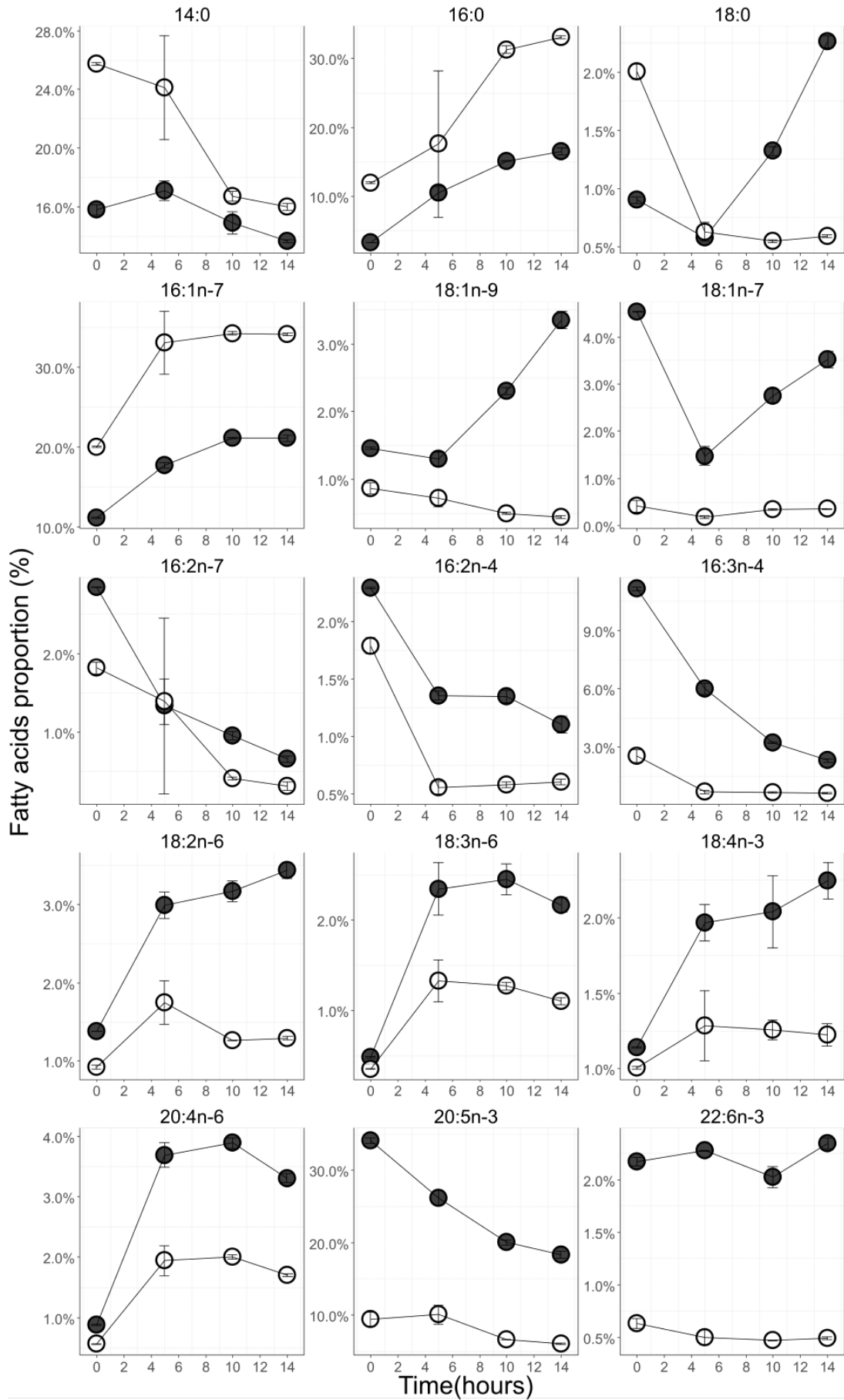


Figure 7: Mean relative proportion (in % \pm SD) of the primary fatty acids (>1% of total fatty acids) of *Chaetoceros muelleri*. Opened dots represent the neutral lipids (NL) and filled dots the polar lipids (PL). The common names of the primary fatty acids are available in Supplementary Files (S1).

Table 3: Relative proportions (in %) of the category of fatty acids of *Chaetoceros muelleri*. Total fatty acids (TFA) represents the sum of all fatty acids and includes saturated fatty acids (SFA), monounsaturated fatty acids (MUFA), polyunsaturated fatty acids (PUFA) and bacterial fatty acids (BACT: 15:0, 17:0, 21:0, 17:1n-7 and iso15:0). NL stands for neutral lipids and PL for polar lipids. Results are expressed as Mean \pm SD (n=3).

Time (d)	Phase I				Phase II			
	t ₀		t ₅		t ₁₀		t ₁₄	
	NL	PL	NL	PL	NL	PL	NL	PL
SFA	41.2 \pm 0.0	20.7 \pm 0.5	43.2 \pm 7.0	28.9 \pm 1.3	48.8 \pm 0.3	32.6 \pm 1.1	50.3 \pm 0.2	34.0 \pm 1.0
MUFA	31.0 \pm 0.6	19.8 \pm 0.1	35.7 \pm 4.2	21.4 \pm 0.5	35.9 \pm 0.2	26.8 \pm 0.3	35.6 \pm 0.1	28.6 \pm 0.5
PUFA	23.1 \pm 1.2	58.9 \pm 0.6	20.5 \pm 2.9	49.5 \pm 1.6	15.2 \pm 0.0	40.5 \pm 0.9	14.0 \pm 0.2	37.3 \pm 0.7
BACT	7.8 \pm 0.5	0.7 \pm 0.0	1.3 \pm 0.2	0.5 \pm 0.1	0.2 \pm 0.0	0.8 \pm 0.3	0.5 \pm 0.3	0.9 \pm 0.4
TFA (mgC.L ⁻¹)	0.8 \pm 0.0	3.2 \pm 0.2	20.8 \pm 4.8	17.1 \pm 0.6	52.2 \pm 0.8	18.7 \pm 0.8	66.3 \pm 8.9	18.7 \pm 0.6
TFA (pg.cells ⁻¹)	1.7 \pm 0.2	4.1 \pm 0.1	3.5 \pm 0.6	2.3 \pm 0.2	9.2 \pm 0.7	2.3 \pm 0.1	11.8 \pm 1.4	2.3 \pm 0.04

The PERMANOVA analysis conducted on NL and PL fatty acids during Phase I (t₅) and Phase II (t₁₀ and t₁₄) revealed a significant difference between sampling times (t₅, t₁₀, t₁₄) for fatty acid percentage (p < 0.001) but no significant difference between cultures replicates (p > 0.05).

The PCA conducted for total fatty acids and coupled with SIMPER analysis showed a clear difference between culture phases. The first sampling points (t₅ and t₁₀) were located on the negative side of axis 1 while the last sampling points (t₁₄) were on the positive side (Figure 8). Axis 1 was driven on the positive side by fatty acids 14:0, 16:3n-4 and 20:5n-3 and on the negative side by 16:0, 16:1n-7 and 18:1n-9. These fatty acids presented opposite proportion dynamics in PL (increases for 16:0, 16:1n-7 and 18:1n-9 and decreases for 14:0, 16:3n-4 and 20:5n-3) (Table 3). Axis 2 was related to lower proportion fatty acids such as 22:6n-3 and 18:2n-6 (positive side) and 20:4n-6 and 18:3n-6 (negative side) in lower proportions (Figure 8). 16:0 and 16:1n-7 appeared to be significantly and positively correlated (Spearman test: TFA: $\alpha = 0.94$ p-value < 0.0001, PL: $\alpha = 0.87$ p-value < 0.0001 and NL: $\alpha = 0.93$ p-value < 0.0001), as well as 16:3n-4 and 20:5n-3 (Spearman test: TFA: $\alpha = 0.92$ p-value

< 0.0001 and PL: $\alpha = 0.85$ p-value < 0.0001) and 18:3n-6 and 20:4n-6 (Spearman test: TFA: $\alpha = 0.95$ p-value < 0.0001, PL: $\alpha = 0.88$ p-value < 0.0001 and NL: $\alpha = 0.89$ p-value < 0.0001), and finally 20:5n-3 and 14:0 (Spearman test: NL: $\alpha = 0.96$ p-value < 0.0001)

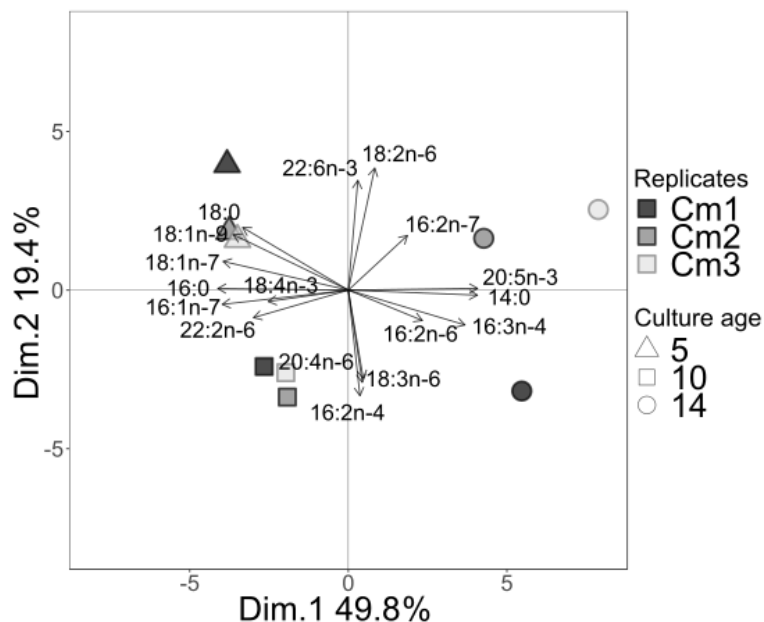


Figure 8: Principal component analysis (PCA) made with % of total fatty acids. Only the fatty acids selected by SIMPER analysis are shown here (explaining 80% of the variability). The colors represent the different culture replicates, and the symbol shapes the culture ages. (Cm = *Chaetoceros muelleri*, n=9)

3.8. Carbon isotopic composition of fatty acids

Carbon isotopic composition ($\delta^{13}\text{C}$ -FA) for the 11 FA studied are presented in Erreur ! Source du renvoi introuvable. Figure 9A. In general, $\delta^{13}\text{C}$ -FA decreased with time (from $-52.9 \pm 1.5\%$ at t_5 to $-58.2 \pm 1.1\%$ at t_{14} in average for NL (ANOVA: p-value < 0.001) and from $-54.1 \pm 2.6\%$ to $-57.2 \pm 1.6\%$ in average for PL (PERMANOVA: p-value < 0.01) (Table 4). $\delta^{13}\text{C}$ -FA of SFA, MUFA, and n-6 PUFA also showed a substantial decrease during the experiment for both NL and PL fractions, while for n-3 PUFA, it was more stable. During Phase I (t_5), $\delta^{13}\text{C}$ -SFA is lower in comparison with $\delta^{13}\text{C}$ -PUFA (Table 4). Overall, the difference between FA categories attenuated with aging culture ranged from -52% to -57% at t_5 and from -56% to 58.6% at t_{14} . During Phase I, $\delta^{13}\text{C}$ of n-3 PUFA was also lighter than $\delta^{13}\text{C}$ of n-6 PUFA (Table 4). $\delta^{13}\text{C}$ of 16:0, 18:2n-6, 18:3n-6 and 20:4n-6 in the PL fraction were always significantly lower than the NL fraction (pairwise Student test, p-value < 0.05) while it was the contrary for 14:0, and 18:4n-3 (pairwise Student test, p-value < 0.05). Isotopic compositions of 16:1n-7, 16:3n-4, and 20:5n-3 in the PL fraction were not significantly different from their isotopic signatures in the NL fraction (pairwise Student test, p-value > 0.05). For the PL fraction, highest $\delta^{13}\text{C}$ -FA were observed at

t₅ for C₁₈ fatty acids (18:1n-9: -50.8 ± 0.2 ‰, 18:2n-6: -51.6 ± 0.1 ‰, 18:3n-6: -51.0 ± 0.7 ‰ and 18:1n-7: -52.0 ± 0.2 ‰) and 16:0 (-51.3 ± 0.2 ‰). At t₁₄ 16:0 and 18:4n-3 were most ¹³C depleted (respectively -58.8 ± 0.0 ‰ and -59.1 ± 0.0 ‰). Regarding the NL fraction, 16:0 and 16:1n-7 were among the least depleted in ¹³C at t₅ (respectively -51.8 ± 0.4 ‰ and -52.6 ± 0.1 ‰) and among the most depleted in ¹³C at t₁₄ (respectively -59.3 ± 0.4 ‰ and -58.1 ± 0.6 ‰).

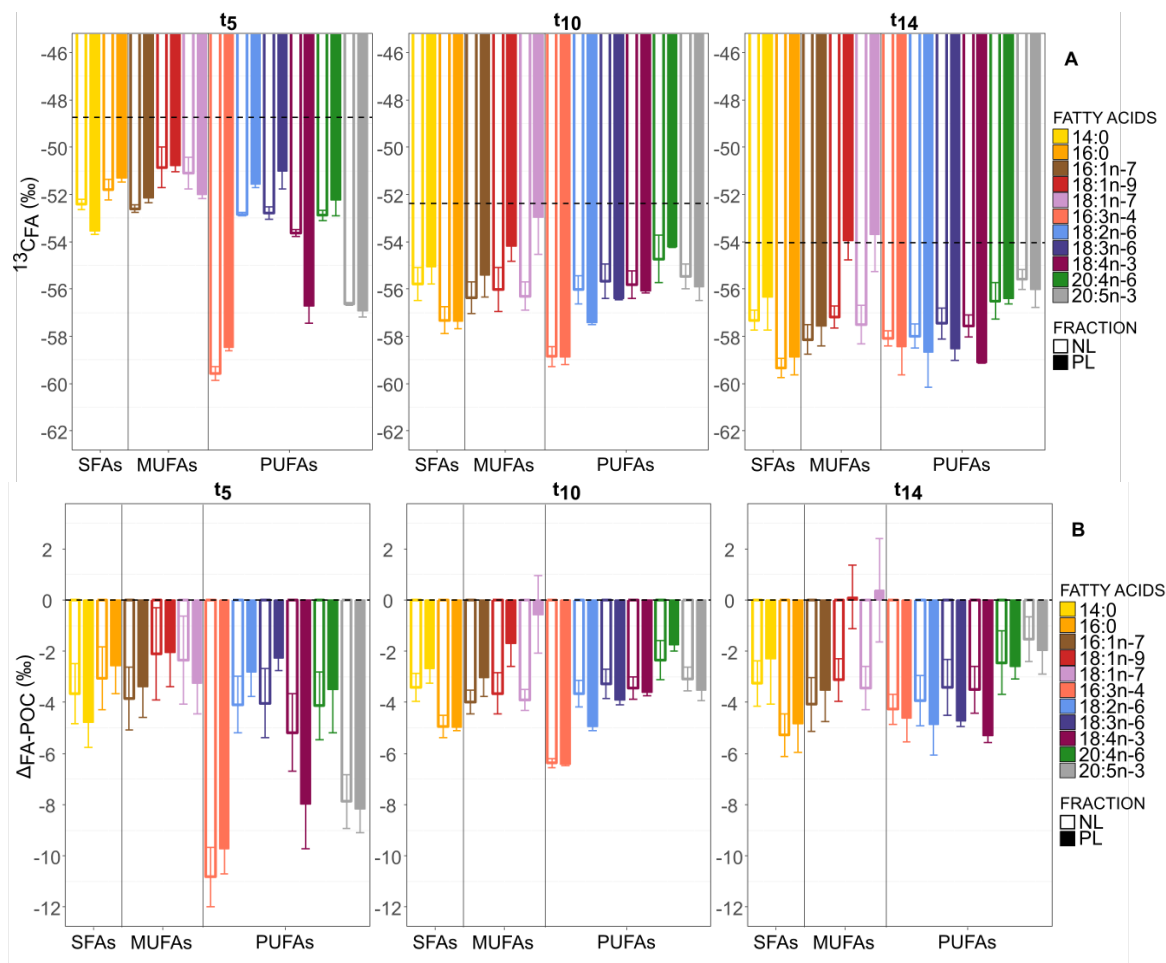


Figure 9: [A] Isotopic ratios ($\delta^{13}\text{C-FA}$) of the eleven main fatty acids studied in *C. muelleri*. The isotopic composition of particulate organic carbon (POC) (dashed line) is considered here as a reference. The empty bars correspond to neutral lipids (NL) and the filled ones to polar lipids (PL). Results are expressed as Mean \pm SD (n=3 and n=2 for polar fraction for all PUFA except 20:5n-3). [B] Comparison of particulate organic carbon and fatty acid isotopic compositions ($\Delta_{\text{FA-POC}}$) in neutral and polar fractions.

Table 4: Time variation of weighted average carbon isotopic composition for each lipid class (saturated (SFA), monounsaturated (MUFA) and polyunsaturated fatty acids (PUFA)) as well as n-3, n-6 PUFA measured for neutral (NL) and polar (PL) fractions. Results are expressed as Mean \pm SD (n=3)

Phase	Phase I						Phase II					
	5		10		14		5		10		14	
Time (d)												
Fraction	NL		PL		NL		PL		NL		PL	
(‰)	m	sd	m	sd	m	sd	m	sd	m	sd	m	sd
SFA	-52.2	0.4	-52.7	1.2	-56.8	1.0	-56.2	1.4	-58.6	1.1	-57.7	1.7
MUFA	-52.6 ¹	0.3	-52.0	0.4	-56.4 ¹	0.6	-55.3	1.1	-58.1 ¹	0.6	-57.0	1.6
PUFA	-55.4 ¹	2.0	-56.0	2.4	-55.5	0.9	-56.0	1.2	-56.4	1.1	-56.6	1.3
n-3	-56.4	0.9	-56.9	0.3	-55.5	0.5	-56.0	0.5	-55.9	0.9	-56.2	1.1
n-6	-52.8	0.2	-51.7	0.7	-55.3	0.9	-55.8	1.5	-57.2	0.9	-57.8	1.3
TOTAL	-52.9¹	1.5	-54.1	2.6	-56.5¹	0.9	-55.9	1.2	-58.2¹	1.1	-57.2	1.6

¹: weighted averages calculated despite lower signal on GC-c-IRMS (< 800 mV) for 18:1n-9, 18:1n-7 & 16:3n-4 (in NL)

The dynamics of 16:3n-4, 18:4n-3 and 20:5n-3 isotopic compositions were overall more stable than other of the FA. 16:3n-4 isotopic composition in both fractions tended to remain relatively stable (-57.4 ± 0.2 ‰ in NL and -58.6 ± 0.2 ‰ in PL). The same observations could be made for 20:5n-3 with, however, a slightly increasing trend between t_5 and t_{10} (average isotopic composition over the studied period: -56.1 ± 0.6 ‰). In NL, 18:4n-3 isotopic signature was progressively more depleted in ¹³C while in PL fraction, its isotopic composition was close to 20:5n-3 at t_5 and t_{10} . Then, 18:4n-3 isotopic composition decreased by 3‰ in PL and by 2‰ in NL between t_{10} and t_{14} .

Isotopic compositions of 16:3n-4 (NL) and 16:1n-7 (PL) as well as 16:3n-4 (PL) and 16:1n-7 (NL) tended to become similar at the end of the monitoring (respectively -58.3 ± 0.2 ‰ and -57.4 ± 0.2 ‰). Similar observations can be made at t_{14} for 20:4n-6 (PL and NL) and 20:5n-3 (PL) (averaging at -56.3 ± 0.2 ‰). After t_5 , 20:4n-6 was always less depleted in ¹³C than C₁₈ PUFA (18:2n-6, 18:3n-6 and 18:4n-3) in both fractions.

Figure 9Erreur ! Source du renvoi introuvable.B compares the isotopic composition of POC and those of FA. For the 11 fatty acids studied, Δ_{FA-POC} were all negative (except 18:1n-9 and 18:1n-7 in PL at t_{14}) corresponding to a ¹³C-depletion in all FA in comparison with POC for both PL and NL. The largest ¹³C difference between POC

and FA was observed at the end of the exponential growth phase (at t_5) for 16:3n-4 (NL: -10.8 ± 1.2 and PL: -9.7 ± 1.0), for 20:5n-3 (PL: -8.2 ± 0.9 and NL: -7.9 ± 1.0) and for 18:4n-3 (PL: -8.0 ± 1.8) while the smallest were noted for 18:1n-7, 18:1n-9 and 20:4n-6 in PL fraction at t_{14} (respectively 0.4 ± 2.0 , 0.1 ± 1.2 ; and -1.7 ± 1.5). Difference between POC and FA isotopic composition remained relatively constant for 14:0 (NL: ANOVA p-value > 0.05), 16:1n-7 (NL and PL: both ANOVA p-value > 0.05), 18:4n-3 (NL: ANOVA p-value > 0.05), 18:2n-6 (NL: ANOVA p-value > 0.05) and 18:3n-6 (NL: ANOVA p-value > 0.05) while they increased for 16:0 in NL and PL (ANOVA p-value < 0.02 and p-value < 0.03 respectively). The difference between POC isotopic signature and those of 20:5n-3 (NL: ANOVA p-value < 0.001 and PL: ANOVA p-value < 0.001) and 16:3n-4 (NL: ANOVA p-value < 0.001 and PL: ANOVA p-value < 0.001) progressively attenuated with time.

4. DISCUSSION

4.1. Dissolved inorganic carbon isotopic signatures due to petrochemical CO₂

The addition of petrochemical CO₂ has drastically modified the isotopic signature of ambient DIC in the culture medium. The initial $\delta^{13}\text{C}$ -DIC of ~ 6 ‰ was progressively replaced by the much ^{13}C depleted carbon of petrochemical CO₂. These changes in $\delta^{13}\text{C}$ -DIC were rapid and took place during the late exponential growth phase suggesting a combined action of algal assimilation (as attested by modification of pH in comparison with the pH of CO₂ control balloon), which removed ambient DIC and continuous supply of depleted petrochemical carbon. This rapid turnover of ambient DIC resulted from high biomass production during the experiment. A simple (and probably oversimplified) POC mass balance model indicated that as soon as t_5 , 93% of produced POC ($9300 \mu\text{mol.L}^{-1}$ or μM) was supported by the added CO₂; the initial DIC level ($\sim 700 \mu\text{mol.L}^{-1}$ or μM) can only explain 7% of the POC production in case of full assimilation. Furthermore, at t_{10} , the mass balance model indicated that 96% of assimilated DIC was of petrochemical origin. Accordingly, the predicted value of $\delta^{13}\text{C}$ -DIC using a binary mixing model was of -28.3 ‰ at t_5 , which was substantially heavier (by 12.7 ‰) than the measured one -15.6 ‰. However, from t_{10} to t_{24} , predicted values of $\delta^{13}\text{C}$ -DIC were quite close to those measured. This deviation observed at t_5 indicated that additional fractionation processes affected the isotopic composition of DIC at the end of the exponential growth phase and were not accounted for with our binary mixing model. This may be related to several parameters as already observed in batch cultures (e.g, Laws, et al. [23]) such as gas dissolution and/or exchange with the headspace, the isotopic equilibrium between DIC species as well as substrate assimilation by the algae since with our experimental setup DIC utilization was largely relative to available dissolved stock. However, resolving these variations was beyond the scope of this study and required further information to be obtained.

4.2. Cellular characteristics and lipid composition changes during *C. muelleri* culture

The cellular characteristics of marine microalgae and their lipid composition varied during the growth of *C. muelleri*. While both NL and PL content increased moderately from t_0 to t_5 , the most remarkable change detected was the sharp increase of NL in terms of both proportion and concentration after t_5 in comparison to PL that remained quite stable (Figure 6). The increase in NL proportion was associated with increases in cell complexity (and size) as attested by SSC (and FSC) temporal dynamics. This was most likely linked to the morphological alterations of shape but also of *C. muelleri* cytoplasmic characteristics [32] in relation to the accumulation of reserve lipids. Such an increase in NL at this age was previously associated with the stationary phase [43-45]. The culture also seemed adjusting its chlorophyll levels as observed by a progressive decrease of FL3 (red fluorescence) from t_5 to t_{24} . Thus, it revealed morphological and physiological variations dependent on culture age during *C. muelleri* growth with t_5 being quite different from $t_{10} - t_{14}$. Variation of lipid fraction concentrations according to culture age was also associated with the modification of fatty acid proportions. As shown in Table 3, Figure 7 and with PCA analysis (Figure 8), C_{16} fatty acids (16:0 and 16:1n-7) and 18:1n-9 in PL increased through time while others such as 20:5n-3, 16:3n-4 and 14:0 decreased. Similar observations can be made in the NL fraction, where 16:0 increased when 20:5n-3 or 14:0 decreased. Observed modifications of morphological, physiological, and biochemical characteristics in relation to *C. muelleri* development may consequently affect carbon fractionation and FA carbon isotopic signatures according to culture age.

4.3. Isotopic compositions of particulate organic carbon and isotopic fractionation during culture growth

The rapid (and robust) decrease observed in the bulk POC isotopic composition ($\delta^{13}\text{C}$ -POC) of *C. muelleri* was closely related to the highly depleted $\delta^{13}\text{C}$ -DIC injected in the ambient medium. The decrease in $\delta^{13}\text{C}$ -POC during the lag and late exponential growth phase (from t_0 to t_5) was especially fast in comparison with the decrease during stationary phase (t_{10} to t_{14}). The isotopic modification introduced in the inorganic substrate was rapidly transferred to the organic compartment during photosynthesis and underlined the tight relationship existing between these two carbon pools. Marine algae are currently experiencing a similar isotopic modification due to the increase of anthropogenic CO_2 in the surface ocean. Anthropogenic CO_2 , mostly derived from fossil fuels with light isotopic composition, tend to decrease the isotopic composition of natural DIC. This current modification is by far of much less amplitude than in our culture. Still, it represents a potential source of variation that is probably already registered in marine organic matter.

Isotopic fractionation in POC obtained in this study ranged between 11.7‰ (Phase I) and 19.0‰ (Phase II) when estimated using $\delta^{13}\text{C-DIC}_{\text{TA}}$ and between 15.3‰ and 24.9‰ when estimated with $\delta^{13}\text{C-DIC}_{\text{M}}$. Overall, these values fall within the range reported in the literature (Table 5). A fractionation value of 17‰ was obtained for *Phaeodactylum tricornutum* [22] and 18.5‰ for *Skeletonema costatum* [10]. Carbon isotopic composition can be influenced by the isotopic composition of the substrate, microalgae physiology, temperature, or enzyme responsible for carbon fixation [8, 46].

Table 5: Fractionation factor (ϵ_P), CO_2 concentrations and growth rates (μ) measured in other studies for diatoms

Taxon	Culture condition	ϵ_P (‰)	$[\text{CO}_{2\text{aq}}]$ ($\mu\text{mol.kg}^{-1}$)	μ (d^{-1})	References
	Chemostat	25.72	34.7	0.5	
<i>Phaeodactylum tricornutum</i>	Nitrate-limited T=22°C	16.76 18.36	2.93 10.27	0.75 1.40	Laws, et al. [12]
	Chemostat	22.22	79.90	0.17	
<i>Porosira glacialis</i>	Continuous light T°C (-0.1 or 2.0°C)	18.15 15.69	23.08 23.00	0.21 0.09	Popp, et al. [19]
	Batch culture				
<i>Phaeodactylum tricornutum</i>	Continuous light Nutrient depleted T=15°C	10-16.7	0-40	1.6	Burkhardt, et al. [22]
	Continuous light, Nutrient enriched T=15°C	12.4 14.1	2.6 25.5	1.7 1.9	Burkhardt, et al. [47]
<i>Skeletonema costatum</i>	Continuous light Nutrient enriched T=15°C	16.7	37.7	1.6	Burkhardt, et al. [47]
<i>Phaeodactylum tricornutum</i>	Continuous light Nutrient enriched T=15°C	12.1 14.3	3.5 25.8	1.6 1.6	Burkhardt, et al. [47]
<i>Thalassiosira weissflogii</i>	Continuous light Nutrient enriched T=15°C	12.1	30.1	0.9	Burkhardt, et al. [47]
<i>Thalassiosira punctigera</i>	Continuous light Nutrient enriched T=15°C	12.1	30.1	0.9	Burkhardt, et al. [47]
<i>Skeletonema costatum</i>	12:12 cycle	18.6			Boller, et al. [10]

F/2 medium

T°=18-22°C

The temperature was not modified during the experiment and so should not be involved in fractionation factor variations. Due to the continuous CO₂ bubbling, in our experimental design, it was assumed that the algae were receiving a sufficient amount of CO₂ by passive diffusion. Thus, CO₂ levels were not a limiting factor to sustain its photosynthesis and development and unlikely required activation of carbon concentrating mechanisms (CCM) known to have a noteworthy kinetic effect on carbon isotopic composition. Laws, et al. [12] also stated that CCM was not perceptible for CO₂ concentration higher than 10 μmol.kg⁻¹.

In addition to the influence of factors mentioned above, it has been shown that carbon fractionation can vary substantially according to RUBISCO types [10, 11, 48]. Five forms (IA, IB, IC, ID, and II) of RUBISCO have been identified in the past years [49]. Form I enzyme consists of eight large and eight small subunits, while form II are dimers of a single subunit homologous to form I large subunit [10]. Forms IA, IB, IC, and ID have been found in marine habitats in cyanobacteria and proteobacteria, eukaryotic green chloroplast or in diatoms, coccolithophores, rhodophytes and some dinoflagellates [10]. The fractionation factor associated with RUBISCO carboxylation, estimated for the diatom *Skeletonema costatum*, was equal to 18.5‰; this was assimilated to the form ID of RUBISCO [10]. However, Popp, et al. [19] and Laws, et al. [12] found higher fractionation factors with the diatom *Porosira glacialis* and *Phaeodactylum tricorutum* (22.2‰ and 25.7‰, respectively). Considering both variations of fractionation factors according to diatom species or culture phase within species, it is difficult to conclude how the respective RUBISCO types, experimental design, or physiology influenced carbon isotopic fractionation in the different studies. It is not clear at this point if these three diatoms species presented the same RUBISCO types. We can only assume that *C. muelleri* studied here possess the ID RUBISCO. Whether *P. glacialis* and *P. tricorutum* have ID RUBISCO remains to be determined. Carbon fractionation appeared to vary intraspecifically as previous studies revealed fairly large differences of fractionation factor within one species such as *Phaeodactylum tricorutum* [12, 19, 47]

4.4. Isotopic composition of fatty acids in neutral and polar lipids

Because of the petrochemical carbon supply, the isotopic composition of total fatty acids of NL and PL fractions was highly depleted, ranging from $-52.9 \pm 1.5\text{‰}$ to $-58.2 \pm 1.1\text{‰}$ and from $-54.1 \pm 2.6\text{‰}$ to $-57.2 \pm 1.6\text{‰}$, respectively, as compared to natural phytoplankton fatty acids (-28 to -36‰) [50, 51]. Total FA isotopic signatures

of both of NL and PL fractions were always more depleted in ^{13}C in comparison with bulk carbon (POC). Other studies previously observed such higher ^{13}C depletion into lipids [13, 28, 52, 53]. Except 18:4n-3 at t_5 and 18:1n-7 and 18:1n-9 at t_{10} and t_{14} , isotopic signatures of FA were similar between NL and PL during the whole experiment, suggesting that structural and reserve lipids in diatoms are connected and used the same pool of newly synthesized fatty acids.

As fractionation varied according to culture ages, the fatty acids isotopic signatures are discussed first for the end of the exponential growth phase (t_5), and second for the stationary phase (t_{10} and t_{14}).

The high ^{13}C depletion and fractionation during Phase I revealed large differences of isotopic compositions between FA. Depending on the importance of the considered fatty acid during growth phase, the FA synthesis efficiency and production may vary. PUFA such as 16:3n-4, 18:4n-3, and 20:5n-3 had more strongly depleted ^{13}C signatures than other fatty acids such as 14:0, 16:0, 16:1n-7, or 18:1n-9. Formation of the latter SFA and MUFA could then be assumed to be faster as their $\Delta_{\text{FA-POC}}$ were low, i.e, their isotopic compositions were close to those of POC. Thus, their productions were associated with less additional isotopic effects and consequently more facilitated, quicker than longer chain PUFA. Taipale, et al. [54] also reported that 16:3n-4 and 20:5n-3 presented a lower $\delta^{13}\text{C}$ than 16:1n-7 or 18:1n-9. Fractionation of 16:3n-4, 18:4n-3, and 20:5n-3 in comparison with POC was above 8‰ (Table 4). These PUFA are produced through complex enzymatic processes involving desaturases and elongase (for 20:5n-3) from their monounsaturated precursors (16:1n-7 for 16:3n-4 and 18:1n-9 for 18:4n-3 and 20:5n-3) [55-58]. However, it is unclear how the isotopic effect occurs during desaturation as carbons are not modified in this enzymatic process. Such isotopic effect(s) of desaturation at the late exponential growth is also supported by the lower depletion of averaged $\delta^{13}\text{C}$ of SFA and MUFA as compared to those of PUFA.

Within PUFA, differences of isotopic composition were observed between n-6 and n-3 PUFA. n-6 PUFA were always less depleted in ^{13}C than n-3 PUFA in both NL and PL fractions (the difference between weighted averages of 4‰ and 5‰ respectively). They seemed to have different roles and regulation at the end of the exponential growth phase. Indeed, n-6 PUFA synthesis appeared faster (lower $\Delta_{\text{FA-POC}}$, less depleted in ^{13}C) than n-4 and n-3 PUFA synthesis (higher $\Delta_{\text{FA-POC}}$, more depleted in ^{13}C). Consequently, efficient synthesis *de novo* of n-4 and n-3 PUFA might be involved in different cellular compartments and physiological roles than n-6 PUFA in *C. muelleri* fitness and growth. 20:5n-3 and 16:3n-4 were identified as essential for diatoms development or stress resistance [59-63].

On the contrary to other PUFA, 18:4n-3 was less depleted in NL than in PL at the end of exponential growth. Both membrane and reserve lipids shared parts of their biosynthesis pathway [55, 56, 64] because they are both relying on the synthesis of diacylglycerol (DAG). DAG is formed from glycerol-3-phosphate (G3P) with a combination of two acyl chains at position *sn*-1 and *sn*-2 of the glycerol backbone. TAG is formed from DAG by an additional acylation at position *sn*-3. Consequently, this fixation of an acyl-chain at position *sn*-3, which is a significant difference between NL and PL pools, might be responsible for an additional isotopic effect discriminating their isotopic composition. At the opposite, fatty acids such as 16:1n-7, 16:3n-4, and 20:5n-3, for which isotopic signatures are very similar between lipids fractions might indicate a closer link.

Regarding the stationary phase (Phase II), there were fewer differences in isotopic signatures between fatty acids. They tended to reach value near -58.2‰ for NL and near -57.2‰ for PL. These observations were associated with lower $\Delta_{\text{FA-POC}}$ values in NL and PL. At the opposite of Phase I, SFA and MUFA ended up being more depleted than PUFA (-58.3‰ versus -56.4‰). During Phase II, 20:5n-3 presented one of the lowest $\Delta_{\text{FA-POC}}$. As mentioned earlier, a low $\Delta_{\text{FA-POC}}$ might correspond to a more active synthesis with less isotopic effects in comparison with the POC signature. We showed that 20:5n-3 proportions were decreasing in both NL and PL fractions during the stationary phase (Phase II). A more active synthesis might be initiated to limit the decrease of this important FA for *C. muelleri*. In parallel, increasing proportion FA such as 16:0 and 16:1n-7, presented isotopic composition with a higher difference in comparison with POC (difference of -4.1‰ to -5.3‰ versus -1.5‰ for 20:5n-3) associated with probable slower synthesis. During Phase II, 20:5n-3 isotopic composition was closer to those of 20:4n-6 than to those of 18:4n-3, which contrasted with Phase I. It is then possible that other synthesis pathways could be activated during Phase II to enhance the production of essential FA of interest (here 20:5n-3). The existence of two different pathways to synthesize 20:5n-3 in diatoms has already been suggested elsewhere [56, 58]. In diatoms, n-3 and n-6 PUFA pathways can be connected in microalgae by desaturation reaction by methyl-end desaturases gathered under the term ω -3 desaturases ($\Delta 15$, $\Delta 17$, $\Delta 19$). These reactions can form n-3 PUFA with n-6 PUFA as precursors [55, 55, 65]. In our study, it concerned the production of 18:4n-3 from 18:3n-6 and 20:5n-3 from 20:4n-6. In both cases, if this metabolic step did occur to form n-3 PUFA during Phase II, the methyl-end desaturation did not present significant fractionation. To ease the understanding of the previous hypotheses, suspected fatty acids synthesis pathways in diatoms are available in Supplementary File (S2).

Finally, the case of 18:1n-9 and 18:1n-7 was interesting at the end of Phase II: a large difference was observed between NL and PL isotopic composition for these fatty acids at t_{14} . While their isotopic compositions in the NL seemed close to those of other fatty acids, their isotopic composition in PL was close to POC signature ($\Delta_{\text{FA-POC}} =$

$0.1 \pm 1.2\text{‰}$ and $\Delta_{\text{FA-POC}} = 0.4 \pm 2.0\text{‰}$ respectively for 18:1n-9 and 18:1n-7). We hypothesized that bacteria might produce 18:1n-9 and 18:1n-7 in PL at this point. Heterotrophic bacteria were previously described as presenting a very low fractionation in comparison with POC [54]. Such origin of 18:1n-9 and 18:1n-7 is supported by the increase of bacteria concentration at the end of the culture (Figure 1B).

5. CONCLUSION

In the present study, fractionation of *Chaetoceros muelleri* POC was shown to vary according to culture phase and cell physiology, as revealed by the negative correlations between fractionation and both FSC/SSC ratio and chlorophyll content. FA isotopic signatures in both reserve (NL fraction) and structure lipids (PL fraction) were overall similar and always more depleted than POC. Proportions and isotopic of individual FA as compared to POC varied according to the culture phase. Some FA (14:0, 16:3n-4, 18:4n-3 and 20:5n-3) were in higher proportion and more depleted (as compared to POC) at the late exponential phase than during the stationary phase while it was the opposite dynamic for 16:0.

Consequently, care must be undertaken while conducting ecological and biogeochemical studies using CSIA on fatty acids as it may provide different information depending on the physiological stages at which phytoplankton cells are collected. As the proportion of reserve lipids (NL) is known to increase when phytoplankton reach the stationary phase, this parameter might be useful to deconvolute and understand isotopic signature recorded in individual FA.

Finally, using petrochemical CO₂ allowed to produce algal biomass strongly depleted in ¹³C (POC isotopic composition ranging from -48.7 to -57.0 ‰ according to culture age) can advantageously be used in ecological and trophic transfer studies as well as for studying biological-related processes such as FA synthesis pathways.

Acknowledgments: We would like to thank Nelly LE GOIC and Christophe LAMBERT for their help with flow cytometry study, Philippe MINER for his support during experimental design development as well as during microalgae cultivation and sampling. Thank to Oanez LEBEAU for her support during isotopic analyses.

Funding: This work was supported by the Université de Bretagne Occidentale (UBO) and Center of Marine Sciences (CMS) of the University of North Carolina Wilmington (UNCW), the Interdisciplinary School for the Blue Planet (ISblue) and the Walter-Zellidja grant of the Académie Française.

Author Contributions: All authors have read and agree to the published version of the manuscript. Conceptualization, Marine Remize, Philippe Soudant and Frédéric Planchon.; methodology, Marine Remize,

Philippe Soudant, Frédéric Planchon, Antoine Bideau, Ai Ning Loh; software, Marine Remize, Fabienne Le Grand, and Antoine Bideau; validation, Marine Remize and Margaux Mathieu-Resuge; formal analysis, Marine Remize and Frédéric Planchon.; investigation, Marine Remize and Margaux Mathieu-Resuge, ; resources, Fabienne Le Grand and Rudolph Corvaisier; data curation, Marine Remize and Frédéric Planchon; writing—original draft preparation, Marine Remize; writing—review and editing, all authors; visualization, Marine Remize; supervision, Philippe Soudant, Ai Ning Loh, Frédéric Planchon, Aswani Voley and Marine Remize; project administration, Philippe Soudant and Marine Remize; funding acquisition, Philippe Soudant Ai Ning Loh and Aswani Voley.

Marine Remize (marine.rem@hotmail.fr) and Philippe Soudant (soudant@univ-brest.fr) take responsibility for the integrity of the work from inception to finished article.

Conflicts of Interest: The authors declare no conflict of interest. The funders had no role in the design of the study; in the collection, analyses, or interpretation of data; in the writing of the manuscript, or in the decision to publish the results.

6. REFERENCES

1. Thompson, P.A., Guo, M.X., and Harrison, P.J. (1992). Effects of variation in temperature. I. on the biochemical composition of eight species of marine phytoplankton. *Journal of Phycology* 28, 481-488.
2. Thompson, P.A., Guo, M.X., Harrison, P.J., and Whyte, J.N.C. (1992). Effects of variation in temperature. II. on the fatty acid composition of eight species of marine phytoplankton. *Journal of Phycology* 28, 488-497.
3. Rousch, J.M., Bingham, S.E., and Sommerfeld, M. (2003). Changes in fatty acid profiles of thermo-intolerant and thermo-tolerant marine diatoms during temperature stress. *Journal of Experimental Marine Biology and Ecology* 295, 145-156.
4. Rousseaux, C., and Gregg, W. (2014). Interannual Variation in Phytoplankton Primary Production at A Global Scale. *Remote Sensing* 6, 1-19.
5. Gruber, N., and Keeling, C.D. (2001). An improved estimate of the isotopic air-sea disequilibrium of CO₂: implications for the oceanic uptake of anthropogenic CO₂. *Geophysical Research Letters* 28, 555-558.
6. Ohkouchi, N., Ogawa, N.O., Chikaraishi, Y., Tanaka, H., and Wada, E. (2015). Biochemical and physiological bases for the use of carbon and nitrogen isotopes in environmental and ecological studies. *Progress in Earth and Planetary Science* 2.
7. Fogel, M.L., and Cifuentes, L.A. (1993). Isotope fractionation during primary production. M.H.E.a.S.A. Macko, ed. (New York: Plenum Press), pp. 73-98.
8. Fry, B. (1996). 13C/12C fractionation by marine diatoms. *Marine Ecology Progress Series* 134, 283-294.
9. Descolas-Gros, C., and Fontugne, M.R. (1990). Stable carbon isotope fractionation by marine phytoplankton during photosynthesis. *Plant, Cell and Environment* 13, 207-218.
10. Boller, A.J., Thomas, P.J., Cavanaugh, C.M., and Scott, K.M. (2015). Isotopic discrimination and kinetic parameters of RubisCO from the marine bloom-forming diatom, *Skeletonema costatum*. *Geobiology* 13, 33-43.
11. Roeske, C.A., and O'Leary, M.H. (1984). Carbon Isotope Effects on the Enzyme-Catalyzed Carboxylation of Ribulose Bisphosphatet. *Biochemistry* 23, 6275-6284.
12. Laws, E.A., Bidigare, R.R., and Popp, B.N. (1997). Effect of growth rate and CO₂ concentration on carbon isotopic fractionation by the marine diatom *Phaeodactylum tricornutum*. *Limnology and Oceanography* 42, 1552-1560.
13. Fang, J., Abrajano, T.A., Comet, P.A., Brooks, J.M., Sassen, R., and MacDonald, I.R. (1993). Gulf of Mexico hydrocarbon seep communities xI. Carbon isotopic fractionation during fatty acid biosynthesis of seep organisms and its implication for chemosynthetic processes. *Chemical Geology (Isotope Geoscience Section)* 109, 271-279.
14. Degens, E.T., Behrendt, M., Gotthardt, B., and Reppmann, E. (1968). Metabolic fractionation of carbon isotopes in marine plankton--II. Data on samples collected off the coasts of Peru and Ecuador. *Deep Sea Research and Oceanographic Abstracts* 15, 11-20.
15. Degens, E.T., Guillard, R.R.L., Sackett, W.M., and Hellebust, J.A. (1968). Metabolic fractionation of carbon isotopes in marine plankton—I. Temperature and respiration experiments. *Deep Sea Research and Oceanographic Abstracts* 15, 1-9.
16. Durako, M.J., and Sackett, W.M. (1992). Influence of carbon source on the stable carbon isotopic composition of the seagrass *Thalassia testudinum*. *Marine Ecology Progress Series* 86, 99-101.
17. Hinga, K.R., Arthur, M.A., Pilson, M.E.Q., and Whitaker, D. (1994). Carbon isotope fractionation by marine phytoplankton in culture : the effects of CO₂ concentration, pH, temperature and species. *Global Biogeochemical Cycles* 8, 92-102.
18. Thompson, P.A., and Calvert, S.E. (1994). Carbon-isotope fractionation by a marine diatom: The influence of irradiance, daylength, pH, and nitrogen source. *Limnology and Oceanography* 39, 1835-1844.
19. Popp, B.N., Laws, E.A., Bidigare, R.R., Dore, J.E., Hanson, K.L., and Wakeham, S.G. (1998). Effect of phytoplankton cell geometry on carbon isotopic fractionation. *Geochimica et Cosmochimica Acta* 62, 69-77.
20. Rost, B., Riebesell, U., Burkhardt, S., and Sültemeyer, D. (2003). Carbon acquisition of bloom-forming marine phytoplankton. *Limnology and Oceanography* 48, 55-67.
21. Benthien, A., Zondervan, I., Engel, A., Hefter, J., Terbrüggen, A., and Riebesell, U. (2007). Carbon isotopic fractionation during a mesocosm bloom experiment dominated by *Emiliania huxleyi*: Effects of CO₂ concentration and primary production. *Geochimica et Cosmochimica Acta* 71, 1528-1541.

22. Burkhardt, S., Riebesell, U., and Zondervan, I. (1999). Effects of growth rate, CO₂ concentration, and cell size on the stable carbon isotope fractionation in marine phytoplankton. *Geochimica et Cosmochimica Acta* *63*, 3729-3741.
23. Laws, E.A., Popp, B.N., Bidigare, R.R., Kennicutt, M.C., and Macko, S.A. (1995). Dependence of phytoplankton carbon isotopic composition on growth rate and [CO_{2(aq)}]: Theoretical considerations and experimental results. *Geochimica et Cosmochimica Acta* *59*, 1131-1138.
24. Sharkey, T.D., and Berry, J.A. (1985). Carbon isotope fractionation of algae as influenced by an inducible CO₂ concentrating mechanism. In *Inorganic carbon uptake by aquatic photosynthetic organisms*, WJ Lucas and Berry Edition Edition., pp. 389-401.
25. Abelson, P.H., and Hoering, T.C. (1961). Carbon isotope fractionation in formation of amino acids by photosynthetic organisms. *Proceeding of the National Academy of Sciences* *47*, 623-632.
26. Park, R., and Epstein, S. (1961). Metabolic fractionation of ¹³C and ¹²C in plants. *Plant Physiology* *36*, 133-138.
27. DeNiro, M., and Epstein, S. (1977). Mechanism of carbon isotope fractionation associated with lipid synthesis. *Science* *197*, 261-263.
28. Monson, D.K., and Hayes, J.M. (1982). Carbon isotopic fractionation in the biosynthesis of bacterial fatty acids. Ozonolysis of unsaturated fatty acids as a means of determining the intramolecular distribution of carbon isotopes. *Geochimica et Cosmochimica Acta* *46*, 139-149.
29. Hayes, J.M. (2001). Fractionation of Carbon and Hydrogen Isotopes in Biosynthetic Processes. *Reviews in Mineralogy and Geochemistry* *43*, 225-277.
30. Schouten, S., Klein Breteler, W.C.M., Blokker, P., Schogt, N., Rijpstra, W.I.C., Grice, K., Baas, M., and Sinninghe Damsté, J.S. (1998). Biosynthetic effects on the stable carbon isotopic compositions of algal lipids: implications for deciphering the carbon isotopic biomarker record. *Geochimica et Cosmochimica Acta* *62*, 1397-1406.
31. Andersen, R.A. *Algal Culturing Techniques*; Elsevier: Amsterdam, The Netherlands, 2005, p. 578
32. Lelong, A., Haberkorn, H., Le Goïc, N., Hégaret, H., and Soudant, P. (2011). A New Insight into Allelopathic Effects of *Alexandrium minutum* on Photosynthesis and Respiration of the Diatom *Chaetoceros neogracile* Revealed by Photosynthetic-performance Analysis and Flow Cytometry. *Microbial Ecology* *62*, 919-930.
33. Seoane, M., González-Fernández, C., Soudant, P., Huvet, A., Esperanza, M., Cid, A., and Paul-Pont, I. (2019). Polystyrene microbeads modulate the energy metabolism of the marine diatom *Chaetoceros neogracile*. *Environmental Pollution* *251*, 362-371.
34. Assayag, N., Rivé, K., Ader, M., Jézéquel, D., and Agrinier, P. (2006). Improved method for isotopic and quantitative analysis of dissolved inorganic carbon in natural water samples. *Rapid Communications in Mass Spectrometry* *20*, 2243-2251.
35. Schimmelmann, A., Albertino, A., Sauer, P.E., Qi, H., Molinie, R., and Mesnard, F. (2009). Nicotine, acetanilide and urea multi-level 2H-, ¹³C- and ¹⁵N-abundance reference materials for continuous-flow isotope ratio mass spectrometry. *Rapid Communications in Mass Spectrometry* *23*, 3513-3521.
36. Lewis, E., and Wallace, D. (1998). CO₂SYS Program developed for CO₂ system calculations. In ORNL/CDIAC-105. (Oak Ridge, Tennessee: Department of Applied Science, Brookhaven National Laboratory), p. 42.
37. Rau, G.H., Riebesell, U., and Wolf-Gladrow, D.A. (1996). A model of photosynthetic ¹³C fractionation by marine phytoplankton based on diffusive molecular CO₂ uptake. *Marine Ecology Progress Series* *133*, 275-285.
38. Freeman, K.H., and Hayes, J.M. (1992). Fractionation of carbon isotopes by phytoplankton and estimates of ancient CO₂ levels. *Global Biogeochemical Cycles* *6*, 185-198.
39. Salvesen, I., Reitan, K.I., Skjermo, J., and Øie, G. (2000). Microbial environments in marine larviculture: Impacts of algal growth rates on the bacterial load in six microalgae. *Aquaculture International* *8*, 275-287.
40. Le Grand, F., Soudant, P., Siah, A., Tremblay, P., Marty, Y., and Kraffe, E. (2014). Disseminated Neoplasia in the Soft-Shell Clam *Mya arenaria*: Membrane Lipid Composition and Functional Parameters of Circulating Cells. *Lipids* *49*, 807-818.
41. Mathieu-Resuge, M., Schaal, G., Kraffe, E., Corvaisier, R., Lebeau, O., Lluch-Costa, S.E., Salgado García, R.L., Kainz, M.J., and Le Grand, F. (2019). Different particle sources in a bivalve species of a coastal lagoon: evidence from stable isotopes, fatty acids, and compound-specific stable isotopes. *Marine Biology* *166*, 89-101.
42. R Core Team (2019). *A language and environment for statistical computing*. Volume 2020, R.F.f.S. Computing, ed. (Vienna, Austria).

43. Courchesne, N.M.D., Parisien, A., Wang, B., and Lan, C.Q. (2009). Enhancement of lipid production using biochemical, genetic and transcription factor engineering approaches. *Journal of Biotechnology* *141*, 31-41.
44. Li, X., Hu, H.Y., Gan, K., and Sun, Y.X. (2010). Effects of different nitrogen and phosphorus concentrations on the growth, nutrient uptake, and lipid accumulation of a freshwater microalga *Scenedesmus* sp. *Bioresource Technology* *101*, 5494-5500.
45. Xu, D., Gao, Z., Li, F., Fan, X., Zhang, X., Ye, N., Mou, S., Liang, C., and Li, D. (2013). Detection and quantitation of lipid in the microalga *Tetraselmis subcordiformis* (Wille) Butcher with BODIPY 505/515 staining. *Bioresource Technology* *127*, 386-390.
46. Michener, R.H., and Kaufman, L. (2007). Stable isotope as tracers in marine food webs: an update. In *Stable isotopes in ecology and environmental science*, 2nd edition Edition, R. Michener and K. Lajtha, eds. (Malden, USA Oxford, UK Carlton, Australia: Blackwell), pp. 22-60.
47. Burkhardt, S., Riebesell, U., and Zondervan, I. (1999). Stable carbon isotope fractionation by marine phytoplankton in response to daylength, growth rate, and CO₂ availability. *Marine Ecology Progress Series* *184*, 31-41.
48. Robinson, J.J., Scott, K.M., O'Leary, M.H., Horken, K., Tabita, F.R., and Cavanaugh, C.M. (2003). Kinetic isotope effect and characterization of form II RubisCO from the chemoautotrophic endosymbionts of the hydrothermal vent tubeworm *Riftia pachyptila*. *Limnology and Oceanography* *48*, 48-54.
49. Tabita, F.R., Hanson, T.E., Li, H., Satagopan, S., Singh, J., and Chan, S. (2007). Function, Structure, and Evolution of the RubisCO-Like Proteins and Their RubisCO Homologs. *Microbiology and Molecular Biology Reviews* *71*, 576-599.
50. Budge, S.M., Wooller, M.J., Springer, A.M., Iverson, S.J., McRoy, C.P., and Divoky, G.J. (2008). Tracing carbon flow in an arctic marine food web using fatty acid-stable isotope analysis. *Oecologia* *157*, 117-129.
51. Kravchuk, E.S., Sushchik, N.N., Makhutova, O.N., Trusova, M.Y., Kalachova, G.S., and Gladyshev, M.I. (2014). Differences in carbon isotope signatures of polyunsaturated fatty acids of two microalgal species. *Doklady Biochemistry and Biophysics* *459*, 183-185.
52. Parker, P.L. (1961). The isotopic composition of the carbon of fatty acids. In *Carnegie Institution of Washington Year Book*, Volume 61, G. Press, ed. (Baltimore, Maryland: Carnegie Institution of Washington), pp. 187-190.
53. Parker, P.L. (1964). The biogeochemistry of the stable isotopes of carbon in a marine bay. *Geochimica et Cosmochimica Acta* *28*.
54. Taipale, S.J., Peltomaa, E., Hiltunen, M., Jones, R.I., and Hahn, M.W. (2015). Inferring Phytoplankton, Terrestrial Plant and Bacteria Bulk $\delta^{13}\text{C}$ Values from Compound Specific Analyses of Lipids and Fatty Acids. *PLoS One* *10*, e0133974.
55. Zulu, N.N., Zienkiewicz, K., Vollheyde, K., and Feussner, I. (2018). Current trends to comprehend lipid metabolism in diatoms. *Progress in Lipid Research* *70*, 1-16.
56. Remize, M., Planchon, F., Loh, A.N., Le Grand, F., Bideau, A., Le Goic, N., Fleury, E., Miner, P., Corvaisier, R., Volety, A., et al. (2020). Study of Synthesis Pathways of the Essential Polyunsaturated Fatty Acid 20:5n-3 in the Diatom *Chaetoceros muelleri* Using ^{13}C -Isotope Labeling. *Biomolecules* *10*, 797.
57. Domergue, F., Spiekermann, P., Lerchl, J., Beckmann, C., Kilian, O., Kroth, P.G., Boland, W., Zahringer, U., and Heinz, E. (2003). New Insight into *Phaeodactylum tricorutum* Fatty Acid Metabolism. Cloning and Functional Characterization of Plastidial and Microsomal Delta 12-Fatty Acid Desaturases. *Plant Physiology* *131*, 1648-1660.
58. Arao, T., and Yamada, M. (1994). Biosynthesis of polyunsaturated fatty acids in the marine diatom, *Phaeodactylum tricorutum*. *Phytochemistry* *35*, 1177-1181.
59. d'Ippolito, G., Cutignano, A., Briante, R., Febbraio, F., Cimino, G., and Fontana, A. (2005). New C16 fatty-acid-based oxylipin pathway in the marine diatom *Thalassiosira rotula*. *Organic & Biomolecular Chemistry* *3*, 4065.
60. d'Ippolito, G., Tucci, S., Cutignano, A., Romano, G., Cimino, G., Miralto, A., and Fontana, A. (2004). The role of complex lipids in the synthesis of bioactive aldehydes of the marine diatom *Skeletonema costatum*. *Biochimica et Biophysica Acta (BBA) - Molecular and Cell Biology of Lipids* *1686*, 100-107.
61. Cutignano, A., d'Ippolito, G., Romano, G., Lamari, N., Cimino, G., Febbraio, F., Nucci, R., and Fontana, A. (2006). Chloroplastic Glycolipids Fuel Aldehyde Biosynthesis in the Marine Diatom *Thalassiosira rotula*. *ChemBioChem* *7*, 450-456.
62. Desbois, A.P., Lebl, T., Yan, L., and Smith, V.J. (2008). Isolation and structural characterisation of two antibacterial free fatty acids from the marine diatom, *Phaeodactylum tricorutum*. *Applied Microbiology and Biotechnology* *81*, 755-764.

63. Parrish, C.C. (2013). Lipids in Marine Ecosystems. *ISRN Oceanography 2013*, 1-16.
64. Maréchal, E., and Lupette, J. (2019). Relationship between acyl-lipid and sterol metabolisms in diatoms. *Biochimie*
65. Monroig, O., and Kabeya, N. (2018). Desaturases and elongases involved in polyunsaturated fatty acid biosynthesis in aquatic invertebrates: a comprehensive review. *Fisheries Science 911-928*.